A Study of the Strong Ground Motions of 26 December 2003 Bam Earthquake: Mw6.5

Mehdi Zaré and Hossein Hamzehloo

Seismologist Research Center, International Institute of Earthquake Engineering and Seismology (IIEES), Tehran, Iran, email: mzare@iiees.ac.ir

ABSTRACT: *The Bam earthquake of 26 December 2003 (Mw6.5) occurred at 01:56:56 (GMT, 05:26:56 local time) around the city of Bam in the southeast of Iran. The Bam earthquake of 26/12/2003 (Mw6.5) has demolished the city of Bam, having a population of about 100000 at the time of the earthquake. The Bam fault-which was mapped before the event on the geological maps-has been reactivated during the 26/12/2003 earthquake. It seems that a length of about 10km (at the surface) of this fault has been reactivated, where it passed exactly from the east of the city of Bam. The fault has a slope towards the west and the focus of the event was located close to the residential area (almost beneath the city of Bam). This caused a great damage in the macroseismic epicentral zone; however the strong motions have been attenuated very rapidly, specially towards the east-and west (fault normal) direction. The vertical directivity effects caused the amplification of the low frequency motions in the fault-normal direction as well as the greater amplitude of the motion on the vertical direction. Two strong phases of energy are seen on the accelerograms. The first comprises of a starting sub-event with right-lateral strike slip mechanism which is located south of Bam. The mechanism of the second sub-event is reverse mechanism. The comparison of observed and simulated ground motion indicates that rupture started at a depth of 8km, south of Bam and propagated toward north.*

Keywords: Bam; Strong Motions; Data processing; Source parameters; Simulation; Stress drop; Velocity; Displacement; SH waves; Sub-events

1. Introduction

The Bam earthquake of December 26, 2003 (*Mw*6.5) demolished the city of Bam in the southeast of Iran, see Figure (1). The earthquake happened at 5:26*am* local time when most of the inhabitants were asleep, that was one of the causes of the great life losses. The number of victims was declared officially to be about than 26500 at the time of the preparation of this article (19/01/2004). More that 50000 people were injured and about 100000 people remain homeless.

The damage was limited to the city of Bam and to a smaller city, Baravat, which is located east of Bam. The inhabitants of the villages located near Bam have left their houses after the earthquake, due to the fear of greater earthquakes (aftershocks) and because of extensive to moderate damage to their buildings.

The city of Bam is well-known for the historical citadel of Arg-e-Bam, which is about 2000 years old. It was almost destroyed in the 2003 Bam earthquake, see Figure (1) [1]. Arg-e Bam is the biggest known mud-brick complex in the world. This historical monument is located on an igneous hill, on the verge of the Silk Road. It has an area of some 240,000 square meters. There is no information about the exact date of its construction but according to Persian history it goes back to 2000 years. It has been repaired several times, and was inhabited until 150 years ago.

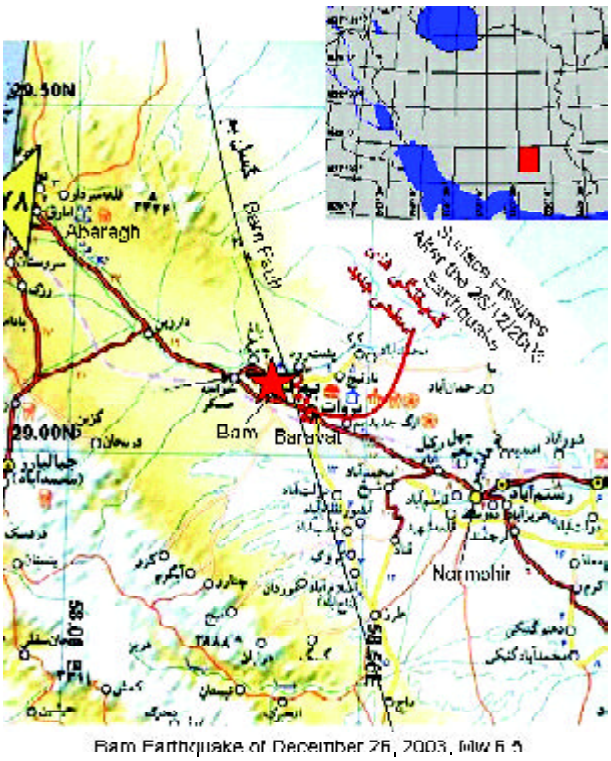

Figure 1. The location map of the Bam earthquake epicentral region in SE of Iran.

Since there is no report of the earthquake occurrence near the city of Bam, in the Iranian historical earthquake catalogue, it seems that it was the first time during the last 2000 years that a disastrous earthquake has taken place due to the reactivation of the Bam fault. The date(s) of the previous earthquake(s) should be determined through paleoseismological studies on the Bam fault.

This paper is prepared to summarize the latest studies of strong ground motions. The strong motions recorded in this event are introduced and most of the paper is focused on the source parameters and on the frequency content of the accelerogram recorded in Bam station, which was located at the Bam city center.

2. Seismotectonics of the Studies Area

The southeast Iran is an active seismic zone, see Figure (2). The Bam city itself had no reported great historical earthquake before the 2003 event [2]. Northwest of Bam, 4 major earthquakes with magnitudes greater than 5.6 have shaken the cities and villages between 1981 and 1998 [3]. The trend of the main faults (including the Bam fault) in this region is North-South, and *NW-SE*, see Figure (1) [1]. These two systems intersect in western Lut area. The NW-SE faults (Kuhbanan and Ravar faults) and the

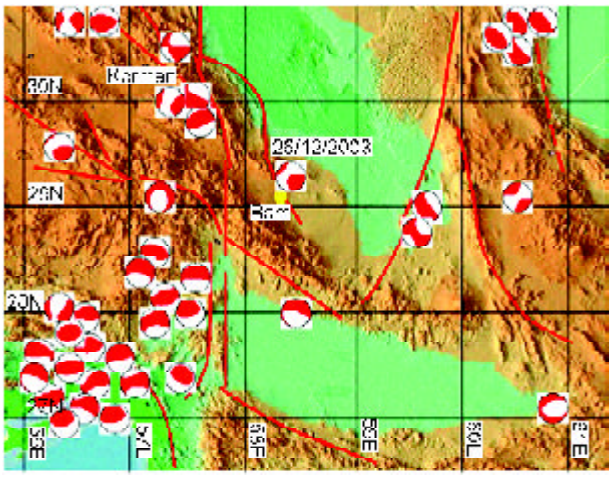

Figure 2. The seismotectonic map of the Bam Region (The base topographic map from USGS Global Digital Data Series [4], focal mechanism from: CMT solutions, Harvard University website [5]).

north-south faults (Nayband, Chahar-Farsakh, Anduhjerd, Gowk, Sarvestan and Bam faults) have determined the order of the north-south structures in the Lut area with the *NW-SE* structures. These intersection zones are the main sources for the disastrous earthquakes. The Gowk fault system is representative for its surface ruptures during 1981, 1989 and 1998 earthquakes as well as a hot spring system nearby Sirch. In the west of Golbaf-Sirch valley, there is the Lut depression, where a vertical topographic offset of more than 4000 meters is evident. Four great earthquakes have shaken the region during the recent years: Golbaf earthquake of 11 June 1981, *Ms*6.6, Sirch earthquake of 28 July 1981, *Ms*7.0, South Golbaf earthquake of 20 November 1989, *mb*5.6 and the North Golbaf (Fandogha) earthquake of 14 March 1998, *Mw*6.6. The Golbaf earthquake of June 11, 1981 has struck the region of Golbaf in the southern parts of the Golbaf valley (with the strike of *N*5-15*E*). This earthquake which was associated with a fault rupture along the Gowk fault resulted in a life loss of 1071 persons. The event caused great damage in Golbaf region. The Sirch earthquake of July 28, 1981 occurred 49 days after the Golbaf earthquake and caused 877 deaths. It seems that it started as secondary faulting along the Gowk fault (*N-S* trend), or was triggered by activation of the Gowk fault in the hidden continuation of the Kuhbanan fault (*NW-SE* trend), in their intersection zone. Such conditions may have lead to the great earthquakes around Sirch in 1877 and 1981 (both with magnitudes greater than 7.0). South Golbaf earthquake of November 20,1989 killed 4 people

injured 45 and caused some damage in Golbaf. Some surface faulting and folding have been reported to be related to this event. During the North Golbaf earthquake of March 14,1998 5 people were killed and 50 injured. The event was associated with surface faulting (about 20km length) in northern Golbaf. The focal mechanism of these earthquakes show the compressional and strike slip mechanisms along the Gowk and Kuhbanan fault systems, see Figure (2).

2.1. Focal Mechanism

The focal mechanism of December 26, 2003 Bam earthquake was reported as strike slip fault (*CMT* solution, Harvard university, web site [5]), see Figure (2), which coincides well with the surface evidence of right-lateral strike slip movement of the Bam fault. The reactivated fault plane had a near north-south direction and sloped towards the west. The focal mechanism reported by Harvard University shows a small reverse component for the fault plane as well. The focal mechanisms reported for the earthquakes which occurred in the region around Bam, see Figure (2), show that most of the earthquakes, which occurred between 1975 and 2003 had strike-slip to compressional mechanisms.

2.2. Bam Fault Scarp

The Bam fault has created a major topographic dislocation in the eastern Bam plain toward Baravat, see Figure (3). This fault scarp shows the vertical displacement of about 10 to 20 meters in different places. It consists of 3 major segments. The total length of such segmented fault system is about 100*km*. The fault escarpment was visited several times after the earthquake but no major earthquake related displacement could be found in its vicinity. The surface fissures, however, are found along this fault zone.

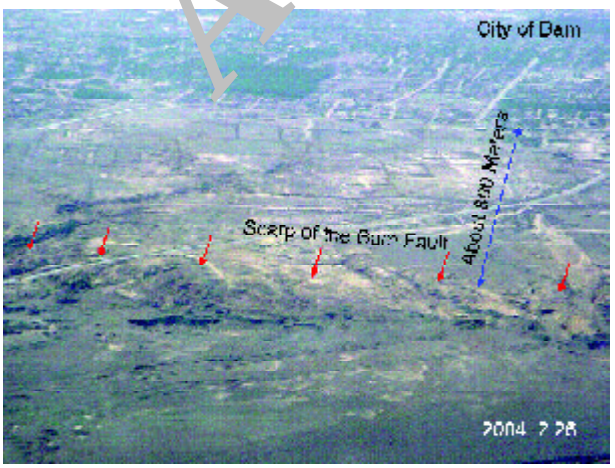

Figure 3. The Bam fault scarp from air (photo by M. Zare, February 2004).

The earthquake induced surface fissures were found in a region between Bam and Baravat and in the vicinity of the Citadel of Arg-e Bam, as well as in the eastern parts of the city of Bam. There was no appearance of the surface displacement on the surface, possibly due to the depth of the earthquake (8*km*) and because of the small dimensions of the source of an earthquake of such magnitude (*Mw*6.5).

2.3. Source Parameters

Based on a preliminary estimation of the seismic moment, a *Mw*=6.5 is assessed for the Bam earthquake. The focal depth of the 2003 Bam earthquake is estimated to be 8*km* and the hypocentral distance for the record obtained at the Bam station is then 12*km* (Based on a *S-P* estimation on the record obtained from the mainshock). The seismic moment is estimated by the author to be based on the fast Fourier transformations using the Haskell method [6] applied to the accelerogram recorded at the Bam station. The stress drop is estimated to be 480 bars.

Section 2.4. (Seismic Gap Is Eliminated)

2.4. Aftershocks

The aftershocks recorded by 25 stations of a temporary network installed by *IIEES* within 3 months after the earthquake are mostly located towards the west of the Bam fault, which is consistent with the slope of the Bam fault towards the west. Most of the focal mechanisms estimated for these aftershocks (for the events having at least 5 well recorded seismograms) show similar mechanisms the *CMT* solution (Harvard University), see Figure (2), for the mainshock. Therefore, the reactivated Bam fault (with a slop towards west and a strike of *NNW-SSE*) was active for 3 months after the mainshock, and most of the aftershocks were focused in the central and southern parts of the Bam fault (east to south of Bam).

3. Recorded Strong Ground Motions

The strong motions of this event were recorded at 22 stations of the national Iranian strong motion network (according to Building and Housing Research Center, *BHRC* web site) [7], see Figure (4). The strong motion records are studied and processed and the preliminary results are presented mostly based on the

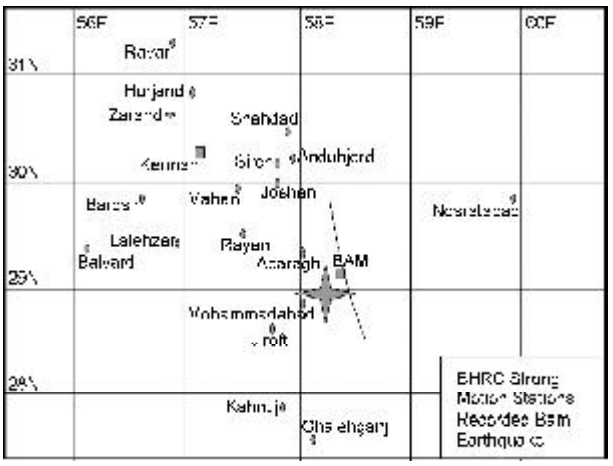

Figure 4. The BHRC strong motion stations that recorded the Bam earthquake.

mainshock and aftershock records obtained at Bam station. All of the strong motion data obtained during the Bam earthquake were recorded by digital Kinemetrics SSA-2 accelerographs. The attenuation of the strong motions was studied based on the records with good signal to noise ratio at 6 stations. The isoseismal map of the region is presented based on the site visits.

3.1. Strong motion Data Processing

The record obtained at Bam station, see Figure (5) -after band-pass filtering between 0.11 and 40[illegible] shows the *PGA* of 775 and 623*cm/sec*[illegible] the east-west and north-south horizontal components, respectively, and 992*cm/sec*[illegible] for the vertical component. This processing is performed based on the estimation of the signal to noise ratio, see Figure (6). The Fast Fourier transformation, see Figure (7) shows more energy at longer periods for the fault normal horizontal component.

A comparison of the *H/V* ratio obtained at Bam station during the mainshock and 13 aftershocks, which occurred in the first 24 hours after the earthquake, see Figure (7) shows very well low frequency amplification between 0.1 and 0.2*Hz* which is evident in the mainshock and it is not evident in the aftershocks. This may be taken as an evidence for

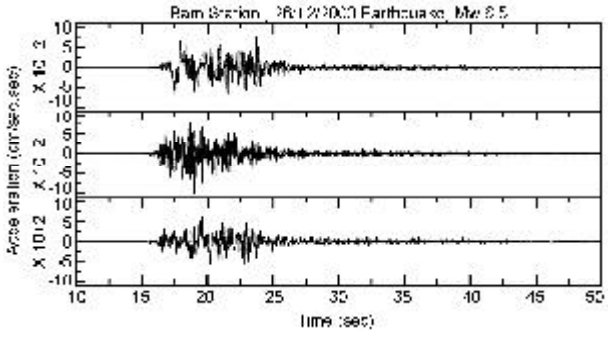

Figure 5. The Bam accelerogram after filtering (between 0.11 and 40Hz).

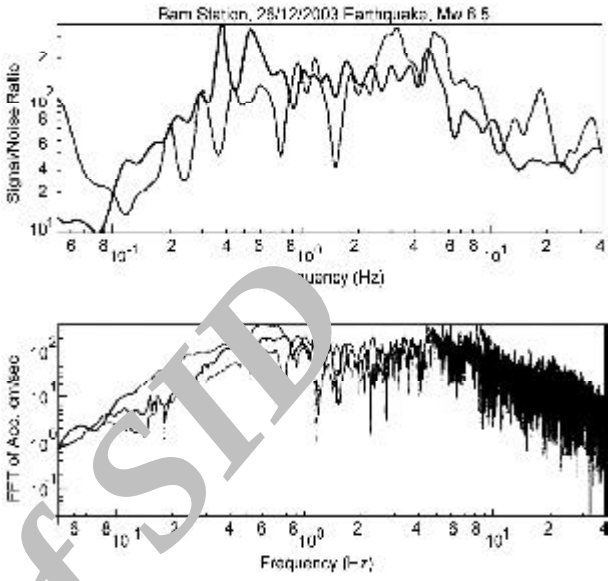

Figure 6. The signal to noise ratio (up) and the FFT of acceleration (down) for the three-components record of Bam.

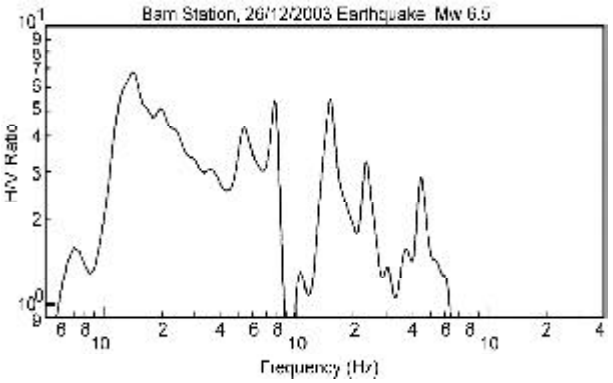

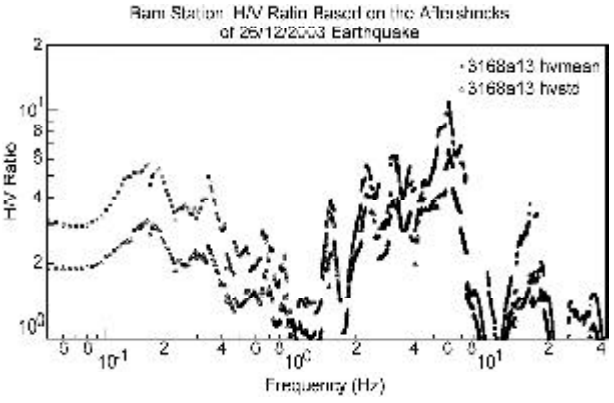

Figure 7. The H/V ratio for a) the mainshock and b) aftershocks recorded in Bam strong motion station.

the vertical directivity effect [18]. The vertical directivity might be explained in the Bam earthquake with the rupture propagation from the depth to the surface with an inclination towards the north. This effect can be assigned to the Bam earthquake fault rupture propagation towards the surface and obliquely towards the north. A strong fault-normal (east-west) motion is created during the mainshock as well. The demolished walls and buildings of Bam are representative for such effects in the up-down (vertical) and east-west directions (fault-normal). The Bam residents that survived the quake explained for the reconnaissance team members that they felt strong up-down displacements during the mainshock. The site class however may be taken for class "3" since the site fundamental frequency was about 2 to 5 *Hz* (equal to a site condition having the average shear wave velocity of about 300 to 500 *m/sec* in the first 30 meters of the deposits, [8]).

The velocity and displacement time-histories of the Bam record obtained based on single and double integration of Bam accelerogram are shown in Figures (8) and (9), respectively. These time-histories show a great pulse specially in the fault-normal component (east-west direction).

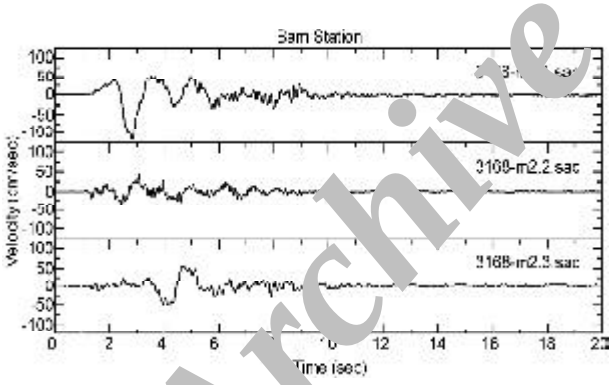

Figure 8 The velocity time-history based on single integration of accelerogram recorded in Bam.

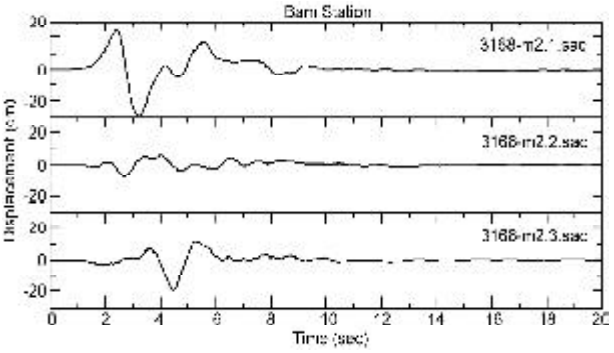

Figure 9. The displacement time-history on double integration of accelerogram recorded in Bam.

The spectral accelerations for 5% damping are shown in Figure (10) for the three-component acceleration recorded at Bam station. The predominant period is the period corresponding to the highest peak in a response spectrum. The response spectra in Figure (10) shows the predominant periods of 0.1 second for vertical and 0.2 second for 2 horizontal components. Figure (10) also shows higher spectral ordinates for the vertical and for the fault-normal components of motion.

The records obtained at the *BHRC* stations around the epicenter, see Figure (4), were processed and the

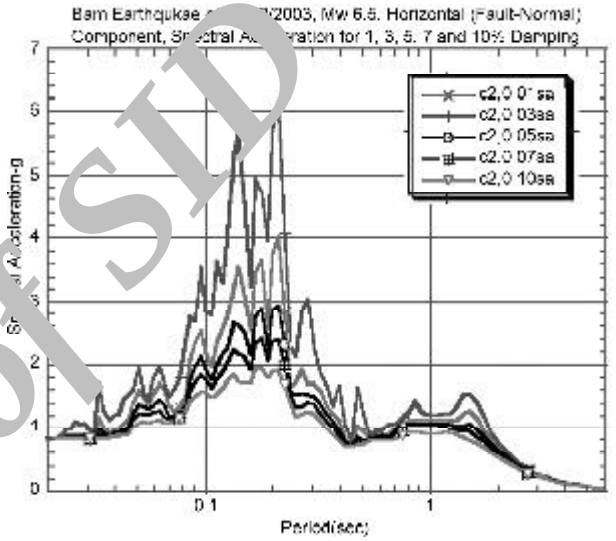

(a)

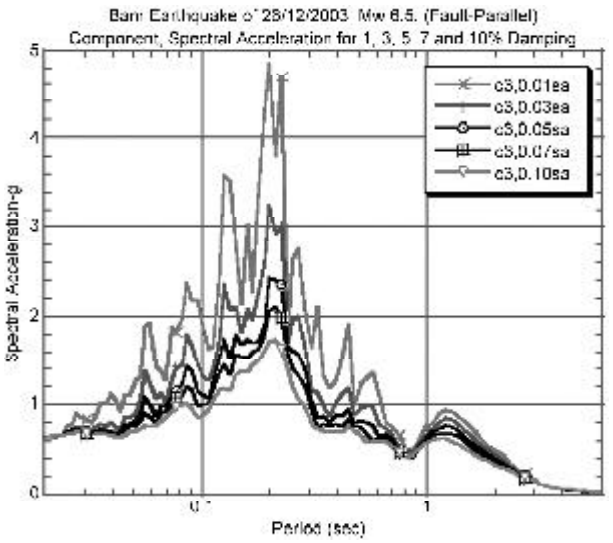

(b)

Figure 10. The spectral acceleration for 1, 3, 5, 7 and 10% damping, the values for 10a) horizontal-fault normal (FN), 10b) fault parallel (FP) and 10c) vertical components are shown. The response spectra for the damping value of 5% are compared for different components in figure 10d.

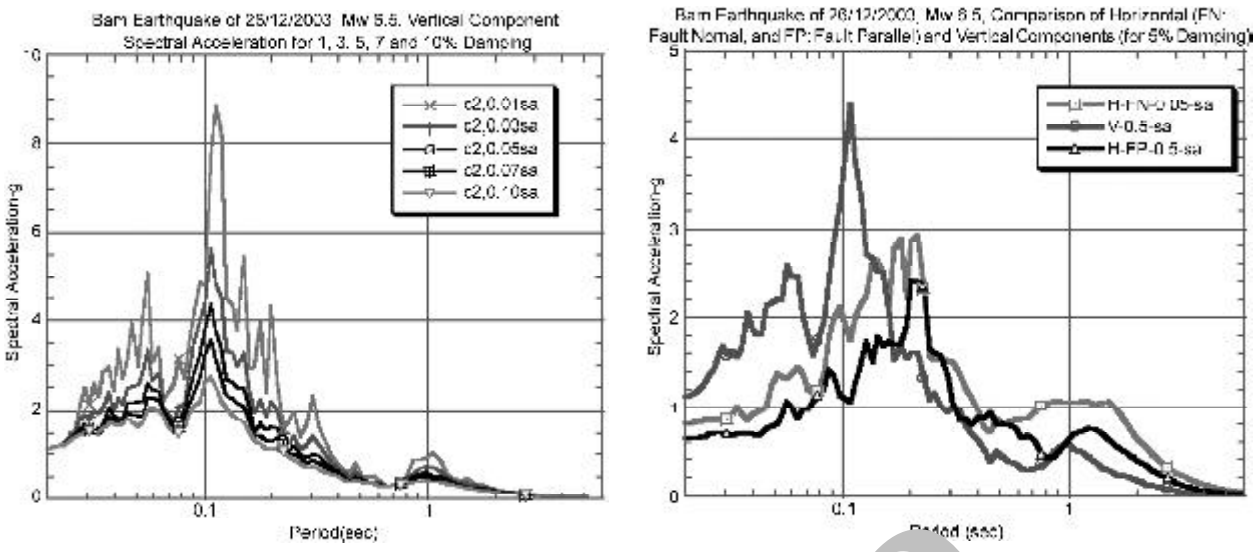

(c)

Figure 10. Continued ...

acceleration time-histories obtained at Bam, see Figure (5), Abaragh, see Figure (11), Mohammadabad-e Maskun, see Figure (12), Jiroft, see Figure (13), Golbaf, see Figure (14), and Sirch, see Figure (15) were selected for the detained strong motion studies. These records were filtered according to their corresponding signal to noise ratio and the band-pass filters are selected are shown in Table (1). Those strong motion records obtained at the stations Arzanjeld, see Figure (16), Cheshmehsabz, see Figure (17), Balvard, see Figure (18), Mahan, see Figure (19), Bardsir, see Figure (20), Hurjand, see Figure (21), Joshan, see Figure (22), Kahnuj, see Figure (23), Kerman-Maskan, see Figure (24), Kerman-Farmandari, see Figure (25), Lalehzar, see Figure (26), Zarand, see Figure (27), Nosratabad, see

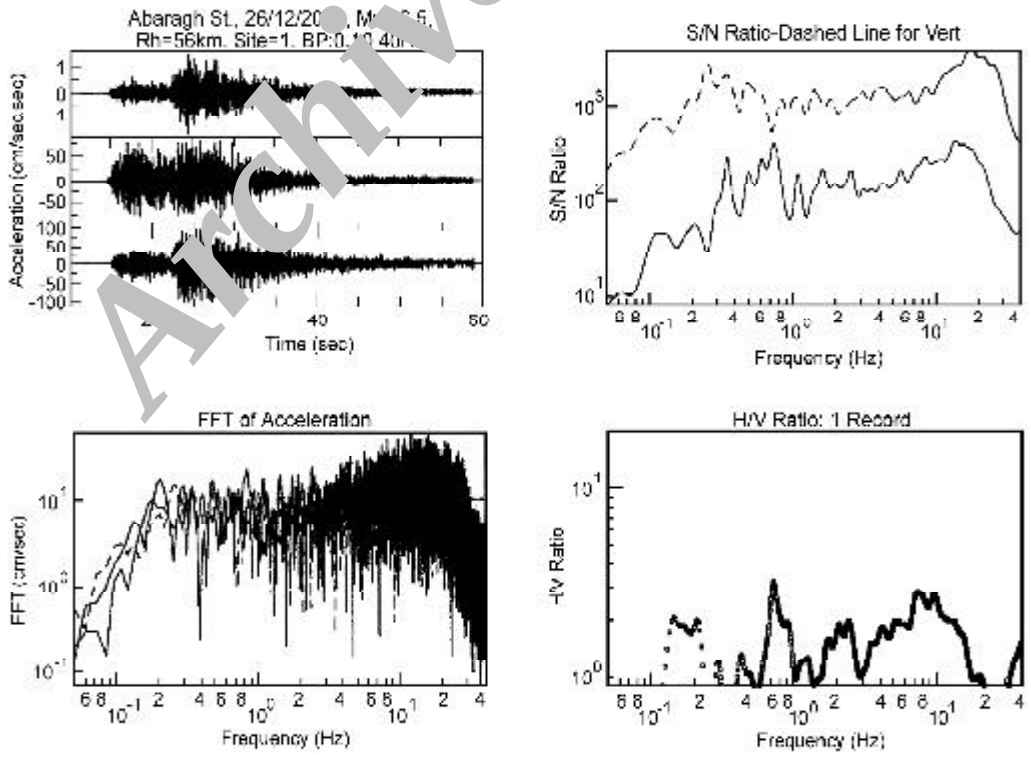

Figure 11. The processing of the record obtained at Abaragh station (56km hypocentral distance): filtered acceleration time-history (above-left); the signal to noise ratio (above-right); the FFT of acceleration before filtering (below-left) and the H/V ratio (below-right).

Figure (28), Ghalehganj, see Figure (29), Shahdad, see Figure (30), Rayen, see Figure (31) and Ravar, see Figure (32) for which the signal to noise ratios are small are presented in the paper but are excluded from the detailed studies of the strong motion parameter.

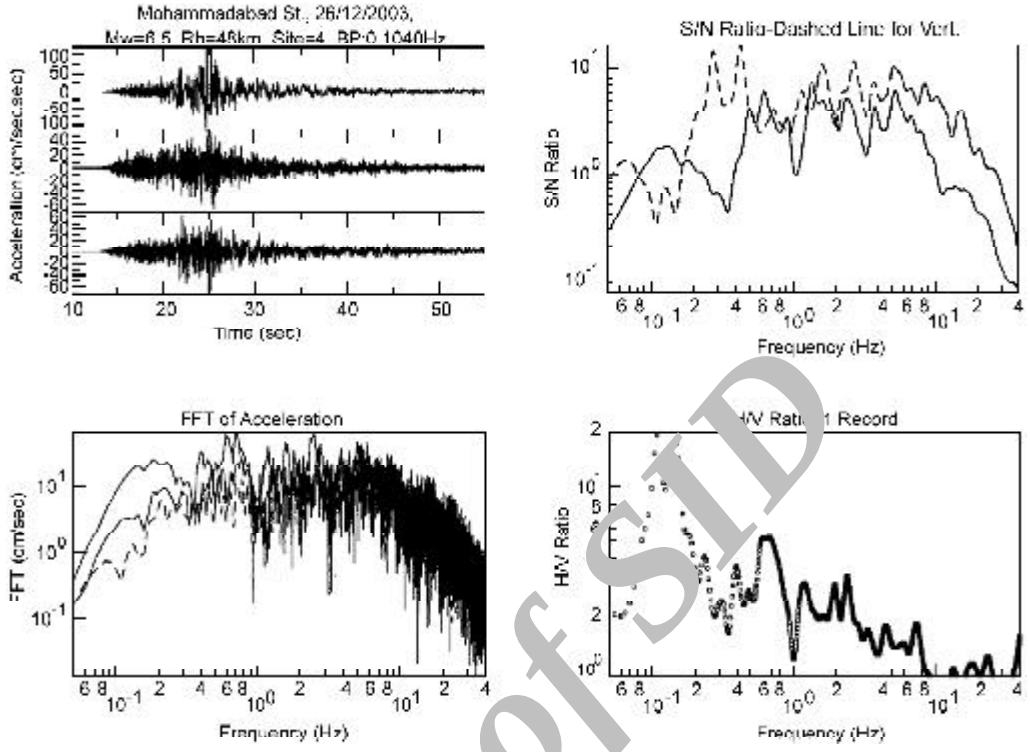

Figure 12. The processing of the record obtained at Mohammadabad-e Maskun station (48km hypocentral distance): filtered acceleration time-history (above-left); the signal to noise ratio (above-right); the FFT of acceleration before filtering (below-left) and the H/V ratio (below-right).

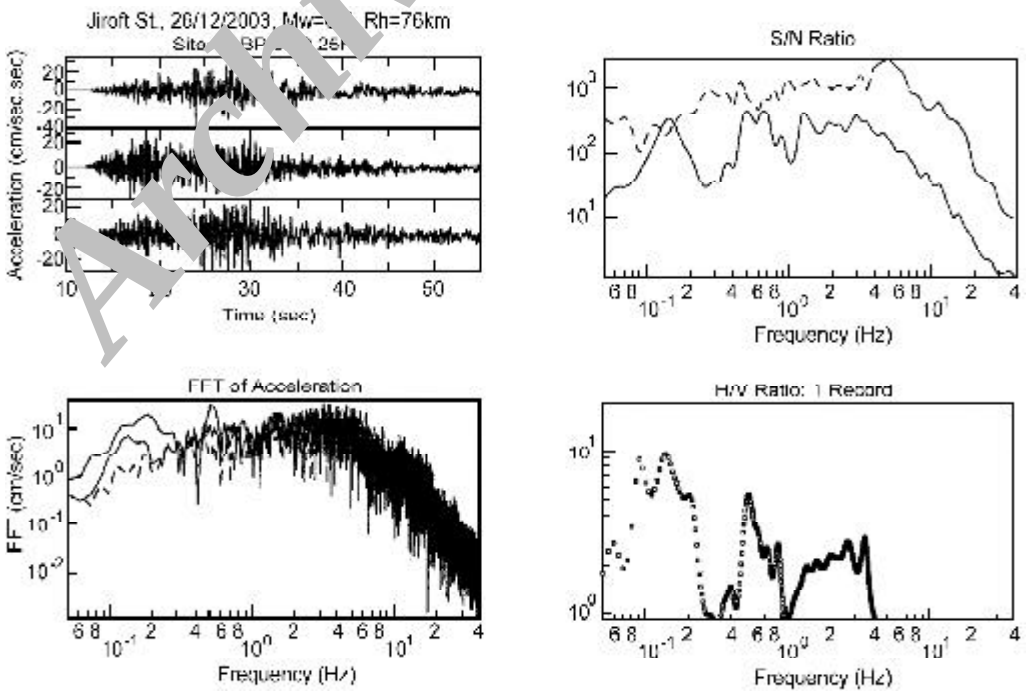

Figure 13. The processing of the record obtained at Jiroft station (76km hypocentral distance): filtered acceleration time-history (above-left); the signal to noise ratio (above-right); the FFT of acceleration before filtering (below-left) and the H/V ratio (below-right).

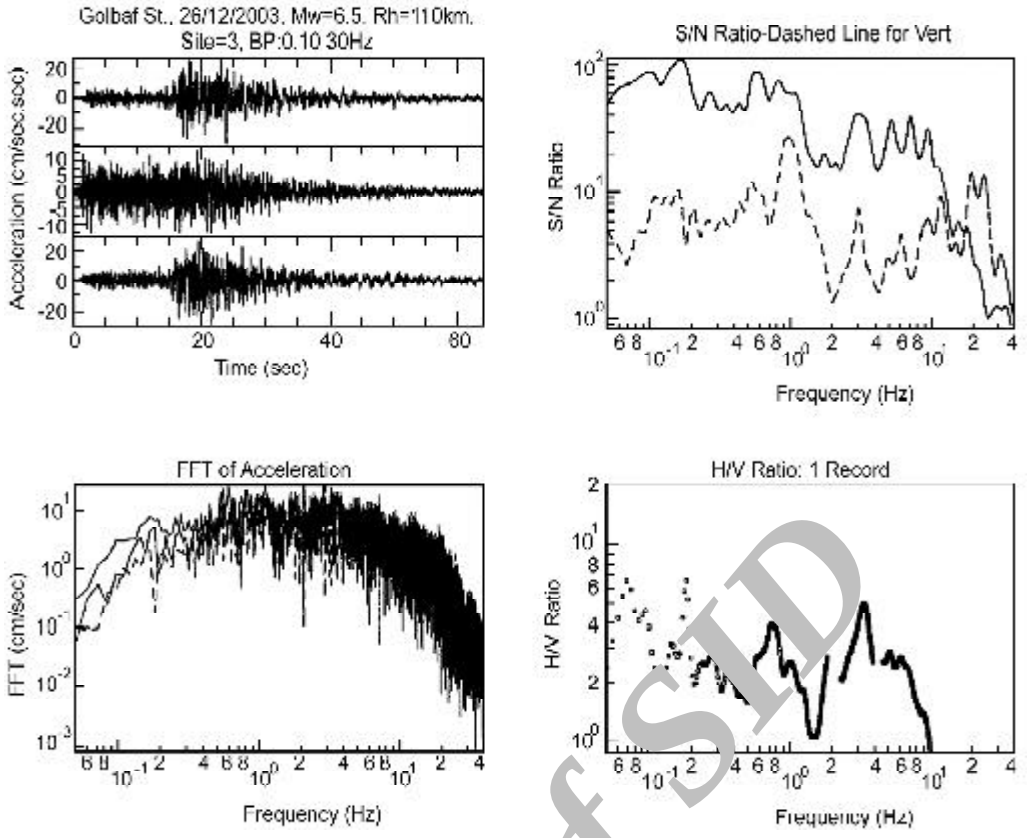

Figure 14. The processing of the record obtained at Golbaf station (1[illegible]km hypocentral distance): filtered acceleration time-history (above-left); the signal to noise ratio (above-right); the FFT of acceleration before filtering (below-left) and the H/V ratio (below-right).

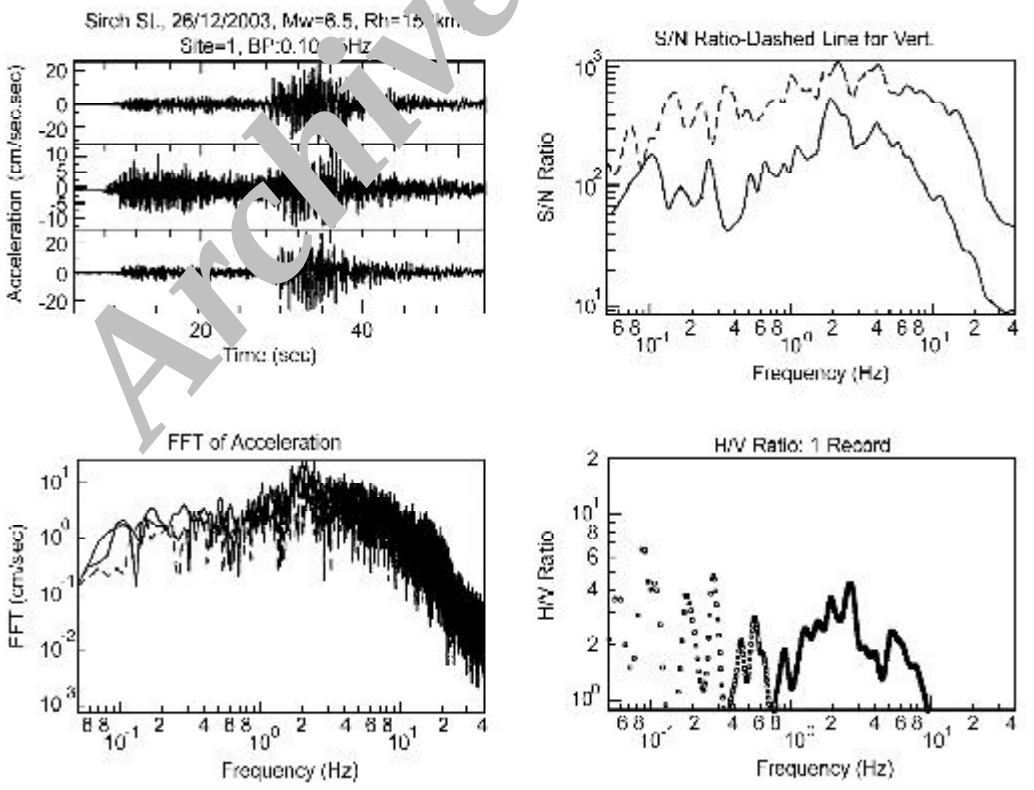

Figure 15. The processing of the record obtained at Abaragh station (152km hypocentral distance): filtered acceleration time-history (above-left); the signal to noise ratio (above-right); the FFT of acceleration before filtering (below-left) and the H/V ratio (below-right).

Table 1. The strong motion parameters estimated for 5 records having better qualities (part-1).

No. of Trace	Record	Station	Lat. N	Long. E	Site	BP Filter (Hz)	HPGA1 (cm/sec^2)	VPGA (cm/sec^2)	HPGA2 (cm/sec^2)	HPGV1 (cm/sec)	VPGV (cm/sec)	HPGV2 (cm/sec)	HPGD1 (cm)	VPGD (cm)	HPGD2 (cm)	Tc (Hz)	Emax -H	Emax -V	Hypocentral Distance (km)
1	3161	Bam	30.24N	57.57E	1	0.1-25	80.2	14	29.2	2.4	1	2.5	0.4	0.2	0.3	0.4	8	15	152
2	3162-1	Mohammad-Abad	29.97N	57.88E	4	0.1-40	120.1	69.2	71	10.4	3.1	3.3	2.1	0.6	0.8	0.4	6	8	48
3	3168-2	Bam	29.12N	58.38E	3	0.11-40	775	392	625	92.3	52.5	72.6	26.4	6.3	15.2	0.2	9	18	12
4	3170-2	Jiroft	28.68N	57.76E	1	0.1-25	99.6	30.5	37.9	3.5	1.3	3.1	0.9	0.1	5.1	0.45	9.5	5	76
5	3176-1	Abarsigh	29.38N	57.97E	1	0.1-40	162.6	83.2	107.7	8.2	8.1	10.2	2.8	2.6	2.2	0.25	18	25	36

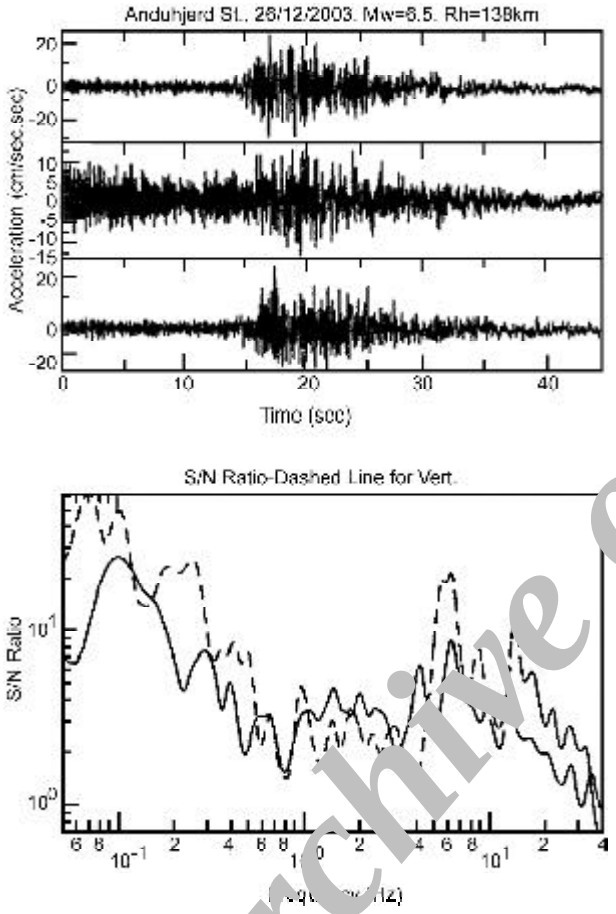

Figure 16. The acceleration time-history (above) and signal to noise ratio for the record obtained at Anduhjerd (138km hypocentral distance).

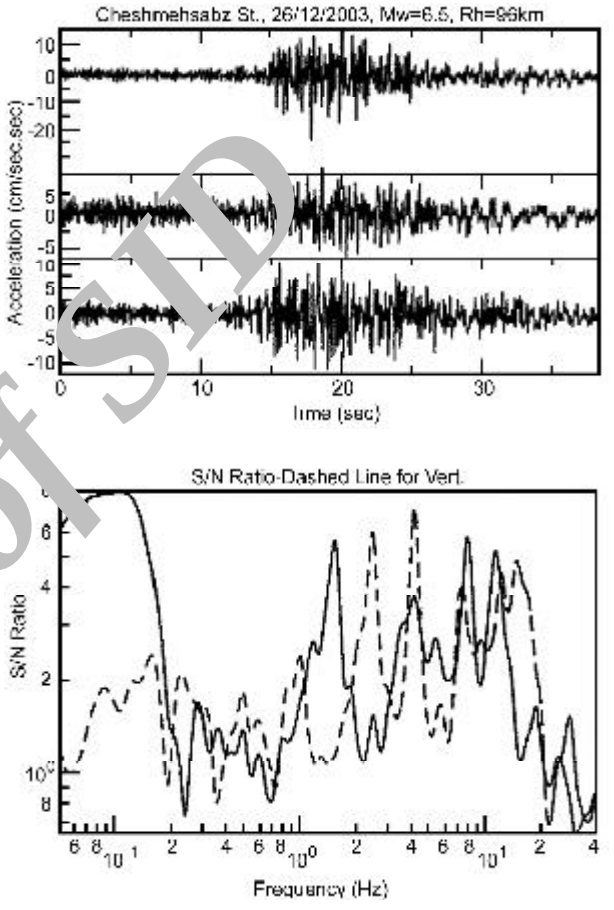

Figure 17. The acceleration time-history (above) and signal to noise ratio for the record obtained at Cheshmehsabz (96km hypocentral distance).

3.2. Strong Motion Parameters

The strong motion parameters estimated for five selected strong motion records are presented in Tables (1) and (2). The estimated parameters for the selected records are explained briefly herein.

3.2.1. Peak Acceleration, Velocity and Displacement

The peak acceleration is the maximum absolute value of acceleration. The peak acceleration provides a useful measure of the strength of the higher frequency components (about 1 to 10*Hz*) of a ground motion. Peak Velocity is the maximum absolute value of velocity. The peak velocity provides a useful measure of the strength of the intermediate frequency components (about 0.5 to 5*Hz*) of a ground motion. Peak Displacement is the maximum absolute value of displacement. The peak displacement provides a useful measure of the strength of the lower frequency components (about 0.1 to 1*Hz*) of a ground motion. These values are presented in the columns 8 to 16 of Table (1).

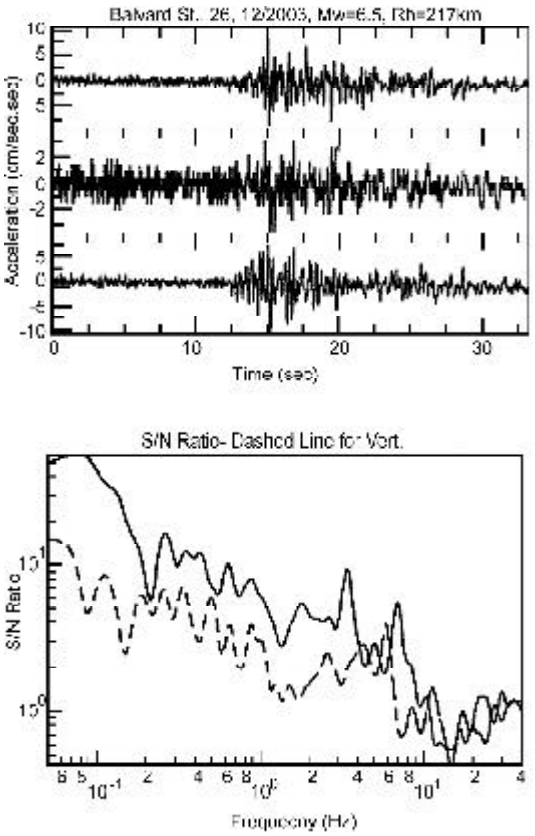

Figure 18. The acceleration time-history (above) and signal to noise ratio for the record obtained at Balvard (217km hypocentral distance).

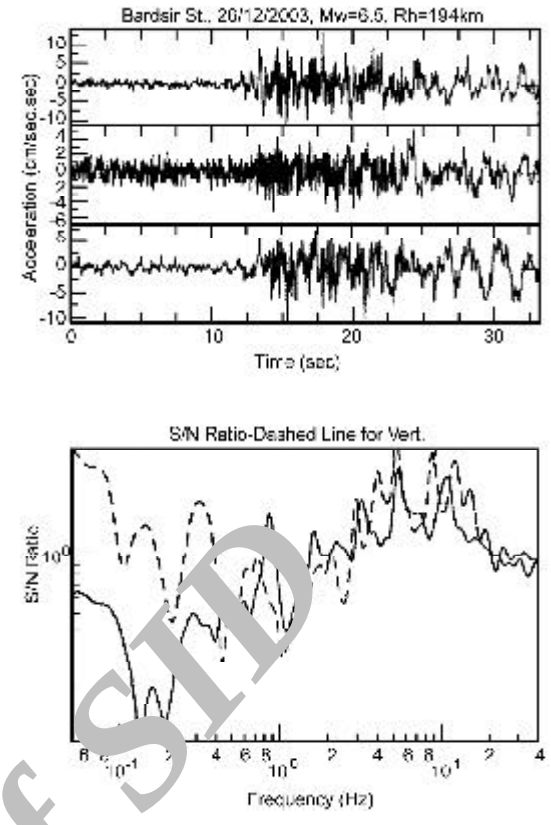

Figure 20. The acceleration time-history (above) and signal to noise ratio for the record obtained at Bardsir (194km hypocentral distance).

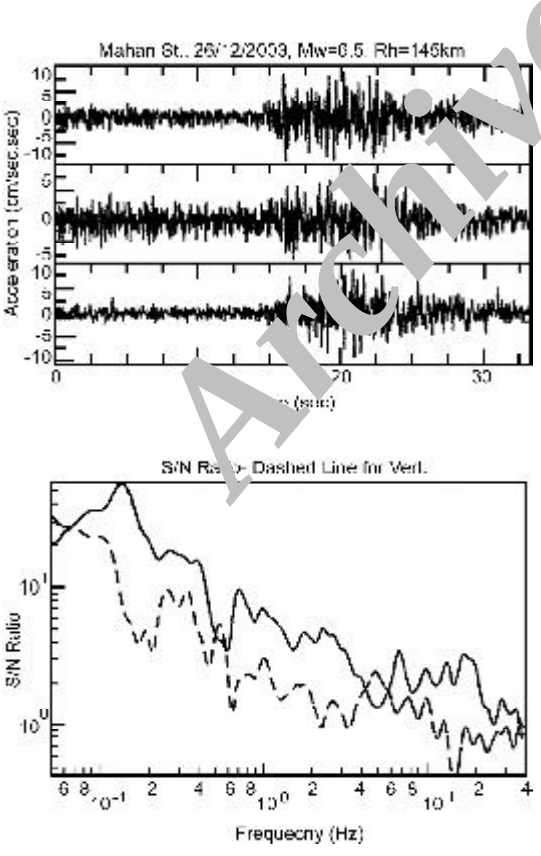

Figure 19. The acceleration time-history (above) and signal to noise ratio for the record obtained at Mahan (145km hypocentral distance).

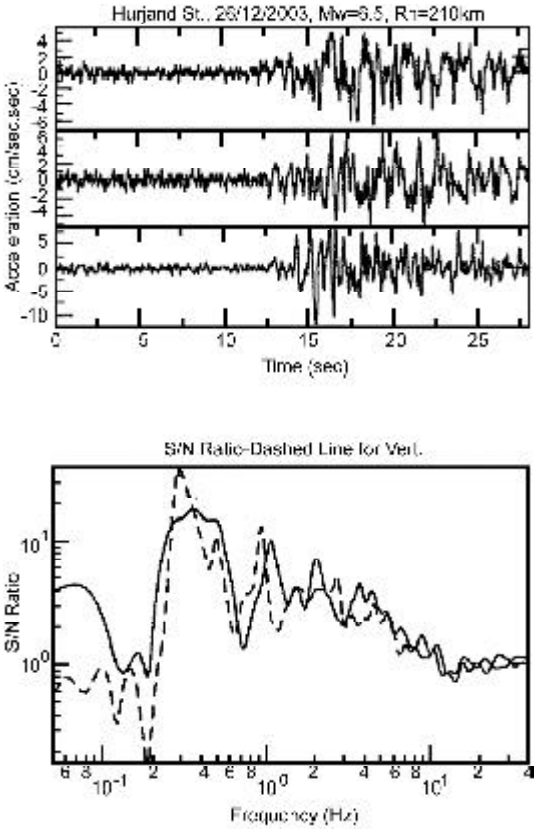

Figure 21. The acceleration time-history (above) and signal to noise ratio for the record obtained at Hurjand (210km hypocentral distance).

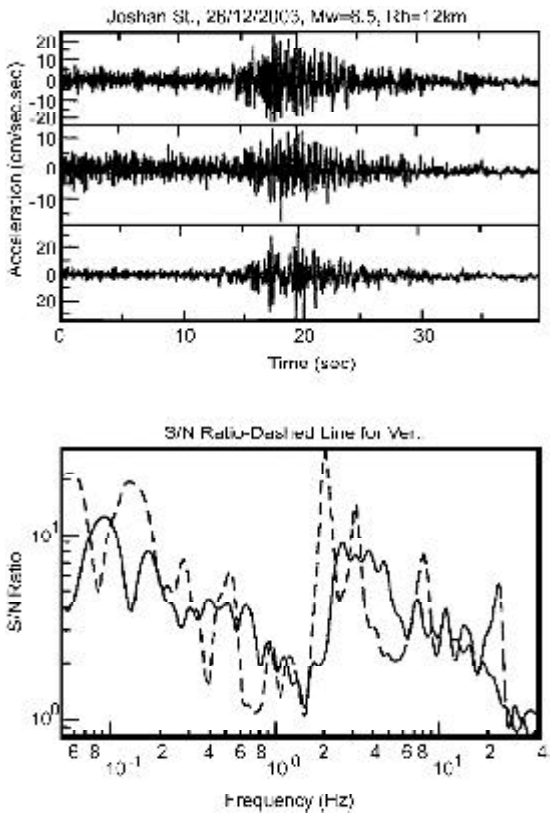

Figure 22. The acceleration time-history (above) and signal to noise ratio for the record obtained at Joshan (129km hypocentral distance).

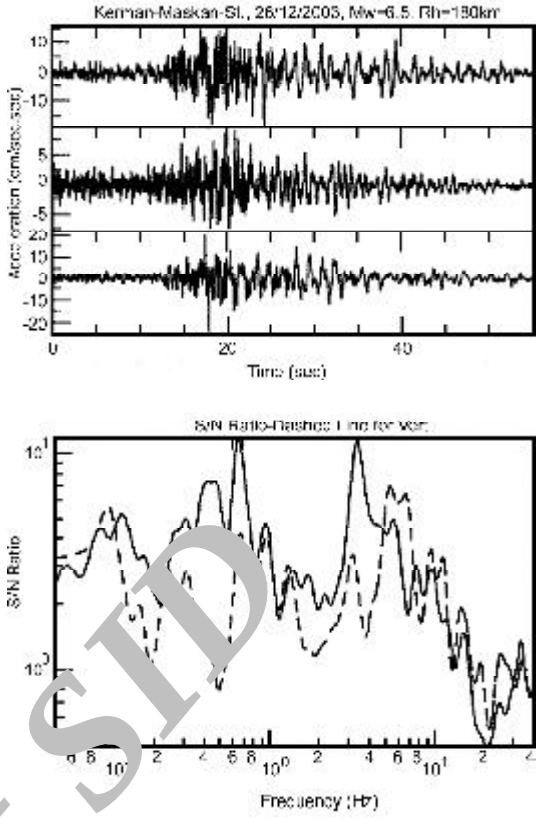

Figure 24. The acceleration time-history (above) and signal to noise ratio for the record obtained at Kerman-Maskan (180km hypocentral distance).

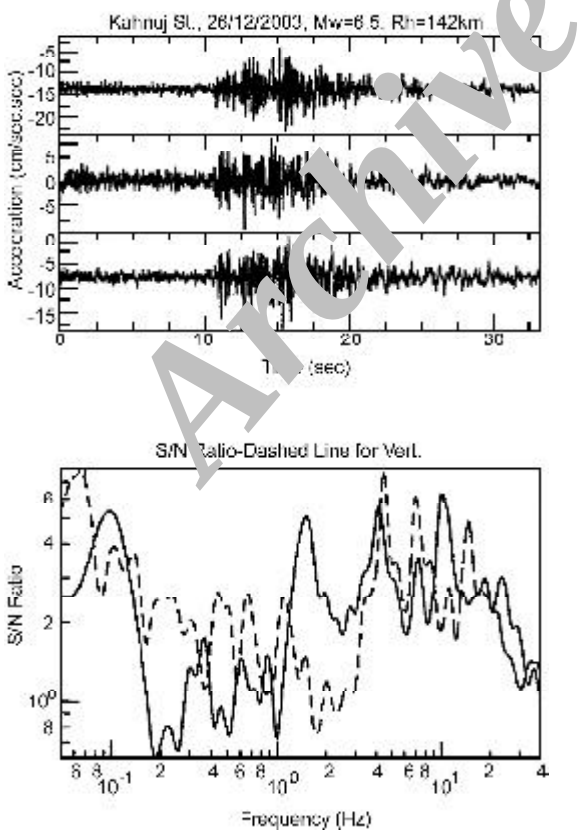

Figure 23. The acceleration time-history (above) and signal to noise ratio for the record obtained at Kahnuj (142km hypocentral distance).

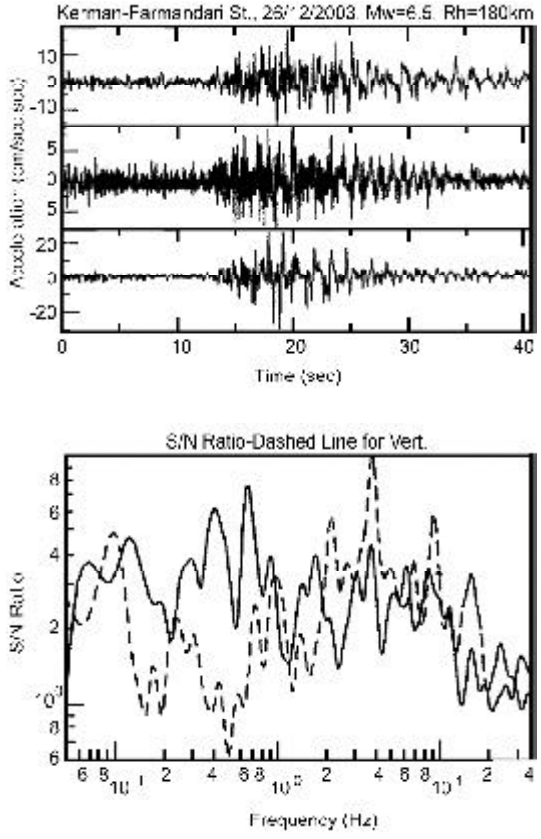

Figure 25. The acceleration time-history (above) and signal to noise ratio for the record obtained at Kerman-Farmandari (180km hypocentral distance).

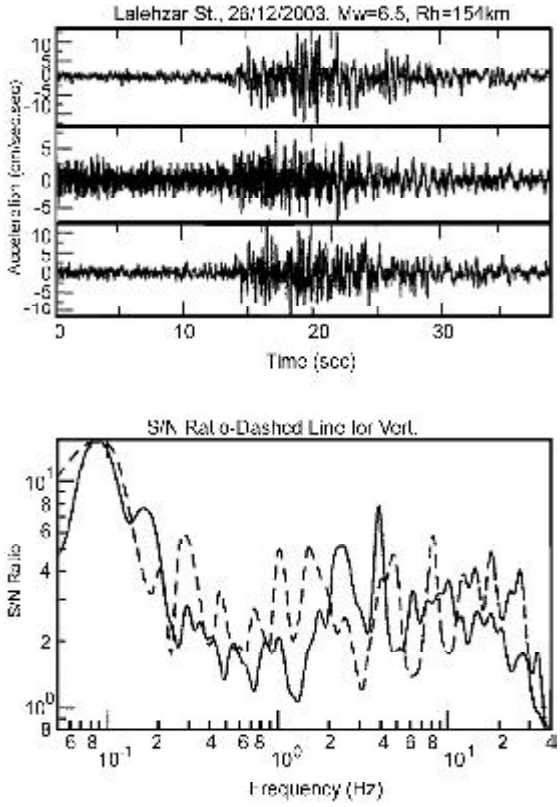

Figure 26. The acceleration time-history (above) and signal to noise ratio for the record obtained at Lalehzar (154km hypocentral distance).

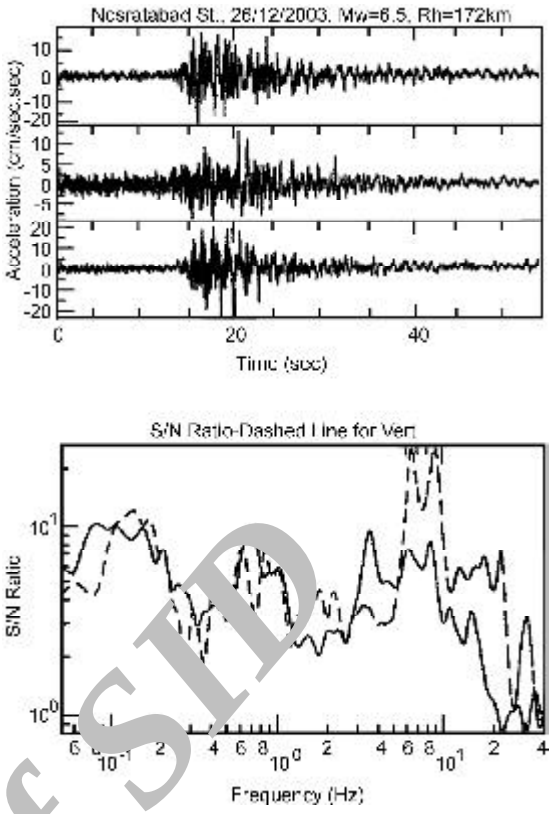

Figure 28. The acceleration time-history (above) and signal to noise ratio for the record obtained at Nosratabad (172km hypocentral distance).

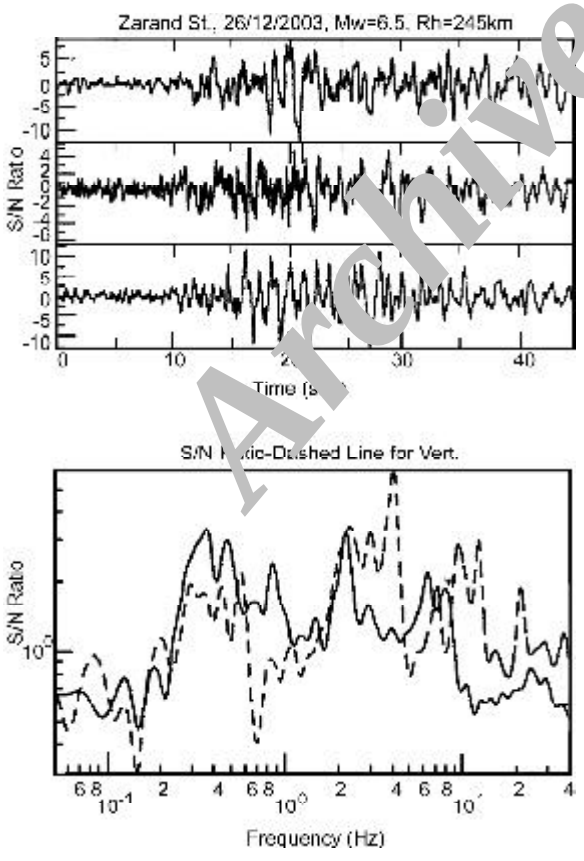

Figure 27. The acceleration time-history (above) and signal to noise ratio for the record obtained at Zarand (245km hypocentral distance).

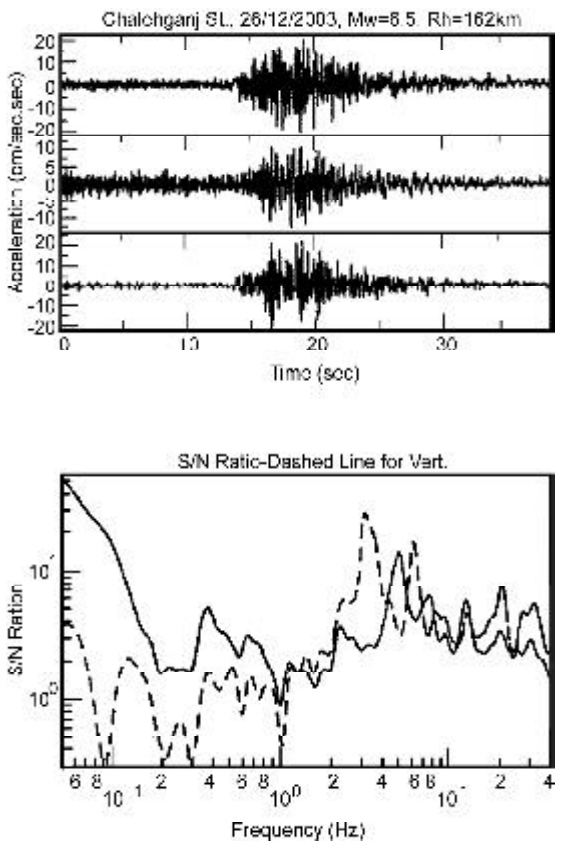

Figure 29. The acceleration time-history (above) and signal to noise ratio for the record obtained at Ghalehganj (162km hypocentral distance).

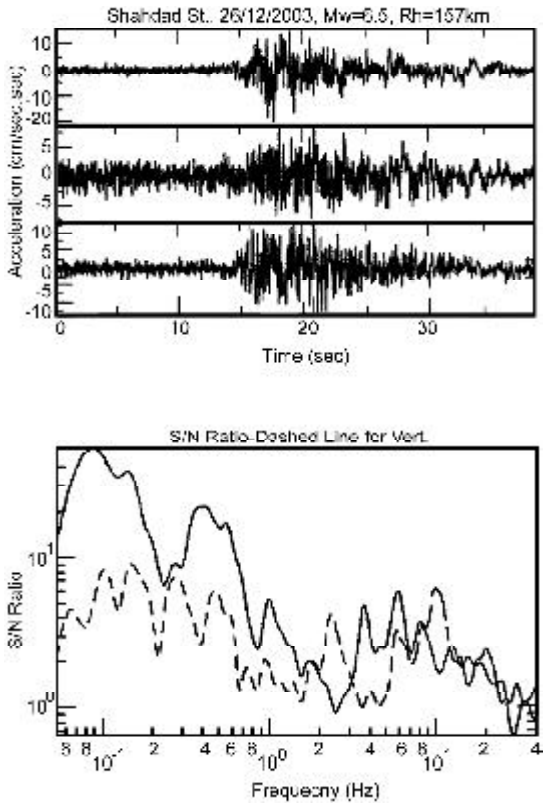

Figure 30. The acceleration time-history (above) and signal to noise ratio for the record obtained at Shahdad (157km hypocentral distance).

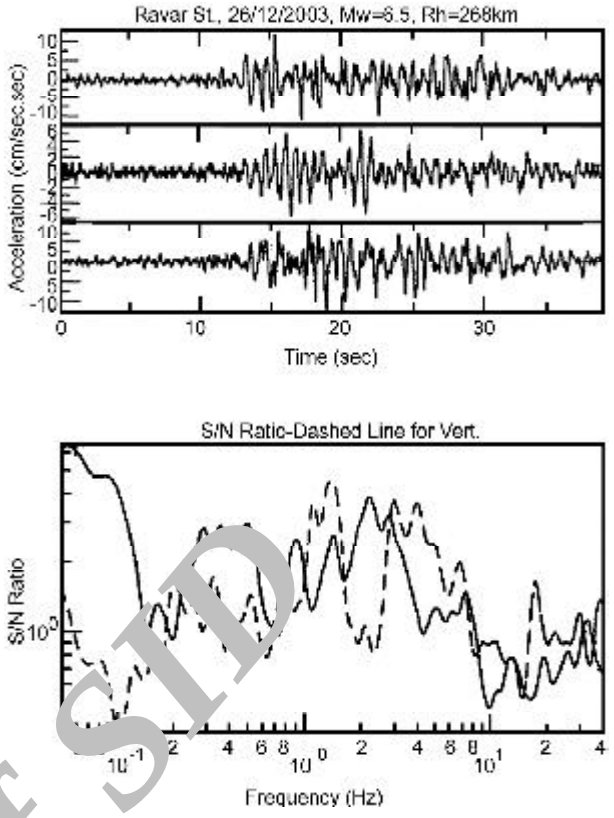

Figure 32. The acceleration time-history (above) and signal to noise ratio for the record obtained at Ravar (268km hypocentral distance).

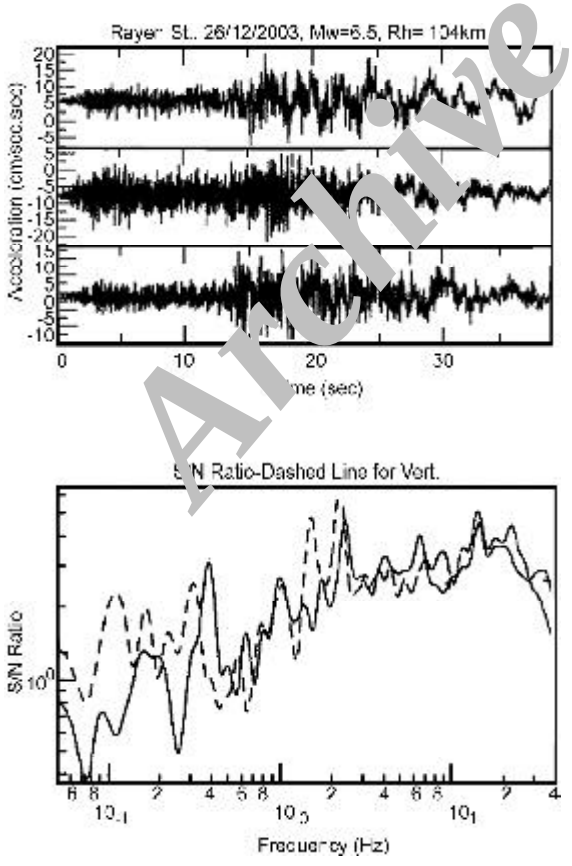

Figure 31. The acceleration time-history (above) and signal to noise ratio for the record obtained at Rayen (104km hypocentral distance).

3.2.2. Root Mean Square (RMS) Acceleration

The *RMS* acceleration is a single parameter that includes the effects of the overall amplitudes of a strong motion record

$$a_{rms} = \sqrt{\frac{1}{Td}\int_{0}^{Td}[a(T)]2dt} \qquad (1)$$

where *Td* is the duration of the motion. Because the integral is not strongly influenced by large, high frequency accelerations (which occur only over a very short period of time) and because it is influenced by the duration of strong motion, the *RMS* acceleration can be a useful parameter for engineering purposes. In the present study we used Trifunac's definition of the duration for computation of the *RMS* acceleration. The estimated values of *RMS* acceleration for the selected records in this study are presented in columns 4 to 6 of Table (2).

3.2.3. Arias Intensity

The Arias Intensity, I_a [9], that is influenced by amplitude, frequency content, and duration, of strong motion. It is defined as

Table 2. The strong motion parameters estimated for 5 records having better qualities (part-2).

No. of Total	Record	Station	Accs-H1 (cm/sec²)	Accs-V (cm/sec²)	Accs-H2 (cm/sec²)	Arias-Int. H1 (cm/sec)	Arias-Int. V (cm/sec)	Arias-Int H2 (cm/sec)	Vel. Spectral Int. H1 (cm/sec)	Vel. Spectral Int. V (cm/sec)	Vel. Spectral Int. H2 (cm/sec)	Duration H1-sec	Duration V-sec	Duration H2-sec
	2-61	Sirch	3.6	3	3.2	2.4	0.7	2	8.2	2.2	8.6	17.3	30.9	17.1
2	3-62-1	Mohammad-Abad	11.5	7.3	7.1	16.6	7	6.8	44.6	13.4	16.9	13.9	20.7	22.6
3	3-68-2	Bam	140.6	135.9	110	99.1	71.8	48.4	304.4	480	515.9	7.7	7.5	8.4
4	21-70-2	Jirofl	6.1	5.6	5.7	3.2	2.8	2.5	16.5	6.7	11.4	23.6	27.6	26
5	21-76-1	Abaragh	19.5	19.3	16.9	36.2	22.1	27	33.2	33.7	35	15	16.4	19.1

$$I_a = \frac{\pi}{2g}\int_0^{\infty}[a(t)]^2 dt \qquad (2)$$

where $a(t)$ is the acceleration time-history. The Arias Intensity has units of velocity and is usually expressed in meters per second. Since it is obtained by integration over the entire duration, rather than over the duration of strong motion, its value is independent of the method used to define the duration of strong motion. The estimated values of Arias intensity for the selected records are given in columns 7 to 10 of Table (2).

3.2.4. Response Spectrum Intensity

The response spectrum intensity $I_a = \frac{\pi}{2g}\int_0^{\infty}[a(t)]^2 dt$ [10] is defined as

$$SI(\xi) = \int_{0.1}^{2.5} PSV(\xi,T)dT \qquad (3)$$

i.e., the area under the pseudo-velocity response spectrum (*PSV*) between period of 0.1 second and 2.5 seconds. The response spectrum intensity is computed here for a structural damping ratio of 5%. It captures overall spectral amplitudes (in the range of primary importance for structures) in a single parameter. The values of velocity response spectral intensity are given in columns 11 to 13 of Table (2) for the selected records.

3.2.5. Trifunac Duration

The Trifunac duration [11] is defined as the time interval between the points at which 5% and 95% of the energy in a ground motion have been delivered. Numerically, it corresponds to the time between the 5% and 95% points on a Husid plot. A Husid plot [$H_n(t)$] shows how the energy of the ground motion is distributed in time. Mathematically, it is a plot of normalized cumulative squared acceleration, i.e.

$$H_n(t) = \frac{\int_0^t [a(t)]^2 dT}{\int_0^{\infty} [a(t)]^2 dT} \qquad (4)$$

where $a(t)$ is the acceleration time history. The estimated durations of selected records are presented in columns 13 to 15 of Table (2).

4. Attenuation of Strong Motions

The Attenuation of strong motions is studied in terms of the processed records obtained at 6 stations (with the accepted level of signal to noise ratios) at Bam, Abaragh, Mohammadabad-e Maskun, Jirof, Golbaf and Sirch. The attenuation of strong motions was studied by Zaré [12] in Iran based on the strong motions recorded between 1974 to1996. A catalogue of Iranian strong motions is published in Bard et al [13]. The attenuation of strong motions recorded at these 6 stations is compared with the values obtained for previous empirical relationships [12] for the *Mw*6.5 earthquake for horizontal and vertical components. The results are shown in Figures (33) and (34) respectively. These figures show very well the coincidence of the estimated and observed values specially for the far-field records.

5. SH Wave Analysis

The analyses of teleseismic and strong ground motion data have been used by different investigators to infer and identify about the complex rupture process and sub-events [14-15]. It is expected that the energy releases from these sub-events will be identifiable in the near field strong motion data and an attempt can be made to study their properties. For this purpose, a method of Sarkar et al [15] has been used to estimate fault plane parameters using strong ground motion data pertaining to *SH* wave only. This method is based on a point source representation and non-linear least square formulation which estimates the strike, dip and rake of the causative fault and a grid

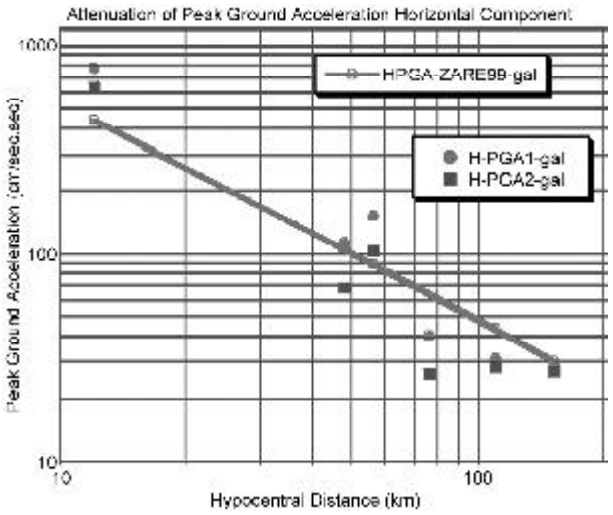

Figure 33. The attenuation of strong motion estimation by Zaré [9] attenuation laws for the horizontal component compared with the observed values in Bam earthquake in 2 horizontal components of 6 selected records.

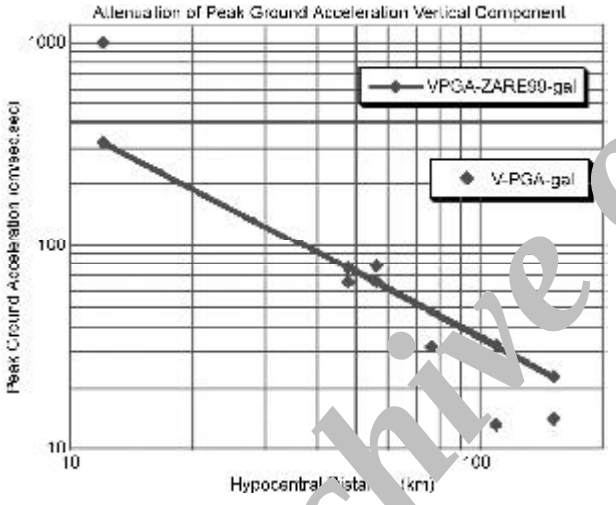

Figure 34. The attenuation of strong motion estimation by Zaré [9] attenuation laws for the vertical component compared with the observed values in Bam earthquake in vertical components of 6 selected records.

search technique that provides separate estimates of the strike, dip and rake. The analysis confines to *SH*-waves because these are minimally affected by crustal heterogeneity [16]. Further, use of *SH*-waves minimizes the need for corrections for the mode conversion at the free surface and other heterogeneities disregarded in the model used here. The spectral amplitudes at various stations are measured at the longest wavelength (lowest frequency) permitted by the data [15]. This is done in order that the point source approximation may be as appropriate as possible.

The observed spectral amplitudes of the acceleration are picked at a common frequency "*f*" on all stations for a particular event, which lies in the flat portions of the spectra and converted into the corresponding values of the spectral displacements. The values are then corrected for geometrical divergence. The corresponding theoretical estimates of *SH*-wave amplitudes of displacement are obtained from the formulae for the radiation pattern of SH-waves in a full space (see for instance) [17-18]. The error function *E* (strike, dip, rake) is written as:

$$E\ (strike,\ dip,\ rake) = \Sigma_i\ (A_{oi} - A_{ti})^2 \qquad (5)$$

Here A_{oi} and A_{ti} denote the observed and theoretical amplitudes of the near field *SH*-wave displacement at the selected frequency at the i^h station. The summation is over all stations that recorded the particular sub-event. The non-linear Newton technique has been used to simultaneously obtain those values of strike, dip, rake which minimize *E* (strike, dip, rake) in the least square sense.

For appropriate selection of *SH*-wave components of the recorded data the radial (*L*) and transverse (*T*) components of recorded acceleration and displacement are suitably rotated so that corresponding estimates along and perpendicular to azimuth direction are obtained. The rotated transverse components provide acceleration and displacement data of SH-waves, recorded at each station. The *SH*-wave accelerogram records for the 2003 Bam earthquake are shown in Figure (35).

5.1. Fault Plane Parameters of Sub-Events

It was observed in Rudbar-Manjil earthquake that strong ground motion data exhibits three strong phases which were interpreted to be related to three asperities [15]. It is expected that the energy releases from these sub-events will be identifiable in the near

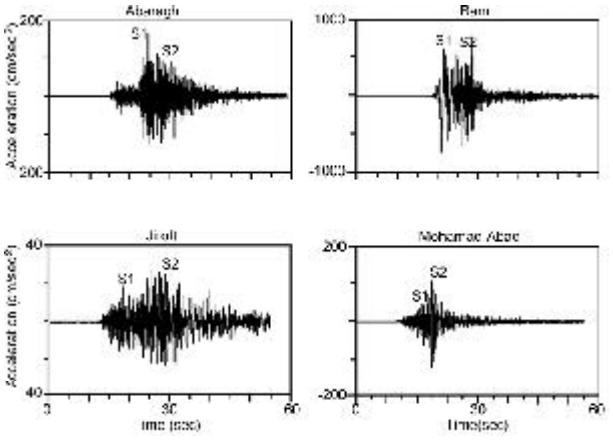

Figure 35. The SH- wave accelerogram records from the four stations of strong motion array.

field strong motion data and an attempt can be made to study their properties. For this purpose, we rotate the observed horizontal component accelerograms appropriately and derive the transverse component accelerograms. These approximately represent the *SH*-wave accelerograms. We next identify the strong phases on these derived accelerograms as signatures of the sub-events. Our assumption here is that a particular phase recorded at a station represents the radiation from the related asperity on the fault. We next consider each strong phase, available from those particular accelerograph stations that recorded it distinctly and the corresponding *SH*-wave spectral amplitude data, in an ensemble. We compensate for geometric divergence, anelastic attenuation, and free surface effect in this data. Then we conduct a non-linear least square inversion on the spectral amplitude in the high fidelity band of the observed spectrum to obtain an average estimate of the strike, dip and rake of the corresponding rupture. In the case of Bam earthquake two strong phases can be seen in recorded strong ground motions, see Figure (35).

In the absence of a common time code, it was not feasible to locate independently the hypocenters of the two sub-events on the basis of the accelerogram data. However, a master event technique was employed to estimate the hypocentral location of the sub-event from where the *S*1 phase of energy was possibly radiated. Generally, a value of two-thirds is usually assumed for the ratio between vertical and horizontal peak accelerations. It has been observed however in recent earthquakes that in near-field there is often a potential for significant vertical component of ground shaking. The Bam station recorded vertical peak acceleration of $992 cm/sec^2$, which is larger than for two horizontal components. It seems at Bam station a strong up-down motion has occurred. This strong up-down motion was also reported by the observers.

At the time of an earthquake, the damage is maximum in the epicentral region, where the ground experiences intense shaking. Therefore, it is assumed here that the chosen master event viz. the sub-event corresponding to the release of the *S*2 phase was located near 58.35° and 29.09° at depth of $8km$ (below the Bam strong motion station). Considering this as location of *S*2 phases, acceleration time histories from the four stations viz. Bam, Abaragh, Mohammadbad and Jiroft, see Table (3) have been used to estimate that the S1 phase of energy was released from 29.02°*N*, 58.30°*E*, at a depth of $8km$ depth, about 8 second before the release of the *S*2 phase of energy.

Table 3. The salient features of recording stations.

Station	Lat.	Long.	Elve.	L/T direction
Abaragh	29.34	57.94	1644	72/162
Bam	29.09	58.35	1094	278/8
Jiroft	28.67	57.74	275	240/330
Mohamad-Abad	28.90	57.89	1961	350/80

The acceleration spectra have been obtained for each of the *S*1 and *S*2 phases using relevant time windows on the appropriately rotated transverse component accelerograms. These spectra were obtained using Fast Fourier Transform (*FFT*) along with a Hamming-Turkey window so as to reduce the effect of data truncation. We performed several variations on the window sizes and placement to confirm the stability of the spectra in terms of their general structure and frequency content. The spectra for *S*1 and *S*2 are shown in Figures (36) and (37), respectively.

The fault plane solution corresponding to the *S*1 sub-event, see Figure (38) estimated using spectra at 4 stations is as follows: strike=174°*N*, dip=85°, rake=

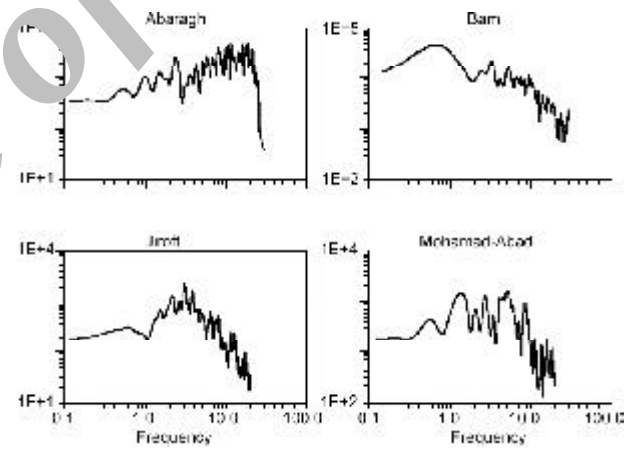

Figure 36. The observed acceleration spectra for S1 sub-event.

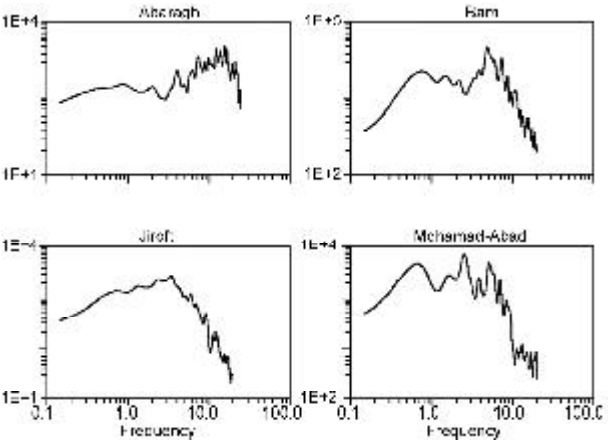

Figure 37. The observed acceleration spectra for S2 sub-event.

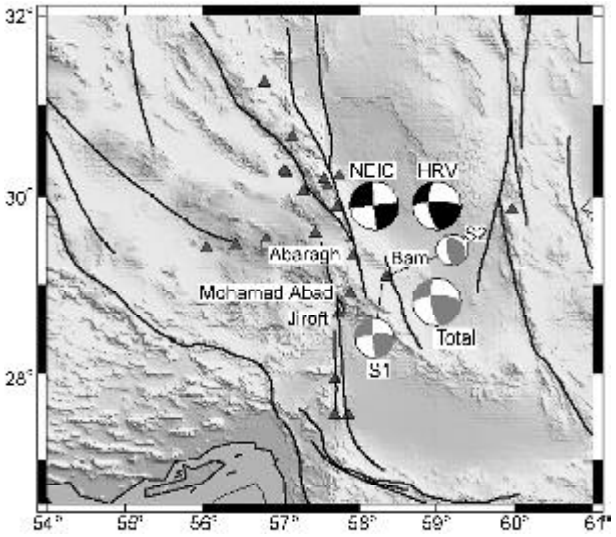

Figure 38. Fault plane solution of two sub-events, total solution from analysis of SH-wave and fault plane solution reported by NEIC and HRV.

170°. The standard error of estimate is 0.50. As mentioned earlier, this event was surmised to have occurred at 29.02°*N*, 58.30°*E*, 8*km*.

For the causative fault of the *S*2 sub-event, see Figure (38), spectral data from four stations have been used to estimate the following parameters: strike=172°*N*, dip=65°, rake=110°. The standard error of estimate is 0.18. We have earlier estimated that the epicenter of this event is located at 29.09°*N*, 58.34°*E* *km* and occurred about 8 seconds after the event *S*1.

The total fault plane parameters, see Figure (38) by considering the SH-wave spectra which includes both *S*1 and *S*2 are as follow: strike=172°, dip=72°, rake=156°. The standard error of estimate is 0.32.

6. Simulation Method

Ground motion recordings from the epicentral region can be of great help in understanding the earthquake process as effects of transmission path are minimal and rupture on the causative fault can be modeled. The strong motion simulation procedures play an important role in complementing traditional approaches to the estimation of strong ground motions. They provide a means of augmenting to the relatively sparse set of strong motion recording close to large earthquake, giving more confidence in the estimation of ground motion characteristics. Simulation procedures also provide a means of estimating the dependence of strong ground motions on variations in specific fault parameters. Simulation procedures provide a means of including specific information about the earthquake source, the wave propagation path between the source and the site and local site response in estimation of ground motion [19].

The strong ground motions have been simulated by considering the fault plane parameters reported by *NEIC*, *HRV* and estimated parameters from *SH*-wave analysis. Strong ground motion has been simulated using a hybrid method, which combine stochastic and Empirical Green's Function (*EGM*) methods. For this purpose small event has been simulated using a stochastic method based on seismological model. This method has been applied to simulate small event because the source size of the small event is small enough to neglect the rupture propagation effect. The Fourier amplitude spectrum of small event, $AS(f,r)$, used in a seismological model [20, 21, 22, 23, 24] can be expressed as a product of a source factor, $S(f)$, a geometrical attenuation factor, $D_{geo}(r)$, a whole path attenuation factor, $D_{An}(f,r)$, upper crust attenuation factor, $P(f)$, and site effects factor, $Z(f)$ as follow:

$$AS(f,r) = S(f).D_{geo}(r).D_{An}(f,r).P(f).Z(f) \qquad (6)$$

The Fourier amplitude spectrum derived from seismological model defines the frequency content of the earthquake ground motion. Then, the synthetic small event is generated using procedure given by Boore [21] and Saiak [25]. Finally strong ground motion from the target earthquake are simulated by applying the *EGF* method of Irikura [26] at selected observation points. The simulated ground motion then is compared with observed ground motion based on the basis of peak ground acceleration, duration and root mean square error (rmse) between observed and simulated response spectra for 5% damping.

A design engineer is always interested in knowing about the maximum force that the structure will experience in the event of an earthquake. For this purpose, the concept of response spectrum is important. In the case of Fourier transform, given a Fourier spectrum, Inverse Fourier Transform (*IFT*) can be performed to determine the accelerogram, which gave rise to that Fourier transform. Although there is a unique response spectra for each time history, the reverse is not true. This implies that inverse mapping of accelerogram from response spectrum is not possible as more than one time histories can be compatible with a response spectrum. In the present study root mean square error is computed using Eq. (7) as measure of goodness for comparison between simulated records from three different models.

$$rmse = \left[\frac{1}{N}\sum_{i=1}^{N}\{(R_{obs_i} - R_{sim_i}) / R_{obs_i}\}^2\right]^{1/2} \qquad (7)$$

where R_{obs} and R_{sim} are the observed and simulated response spectra, respectively. For an objective choice from amongst the many models, the following two criteria are used for choosing the preferred model;

1. The model that gives a maximum number of extracted features (*P.G.A* and duration) that have a less than 10% difference between observed and simulated records i.e., the match for each variable is at least 90%.
2. The model that gives maximum number of stations for which *rmse* is minimum between observed and simulated response spectra.

6.1. Simulation Results

Using modeling parameters of rupture plane, see Table (4) and hybrid simulation method strong ground motion have been simulated at four stations. Strong ground motion at four station have been simulated for three models. First model (M_1) is according to *NEIC* solution. Strike, dip and rake for this model are considered as 174°, 88° and 178°, respectively. The second model (M_2) is based on *HRV* solution. The strike, dip and rake are 173°,63°, and 164°, respectively. The strike dip and rake for the third model (M_3) are considered based on analysis of *SH*-wave as 172°, 72° and 156°. The other modeling parameters, see Table (4) are kept constant for these three models. The simulated and observed records at Bam, Abaragh, Mohamadabad and Jiroft stations for these three models are shown in Figures (39) to (41). The

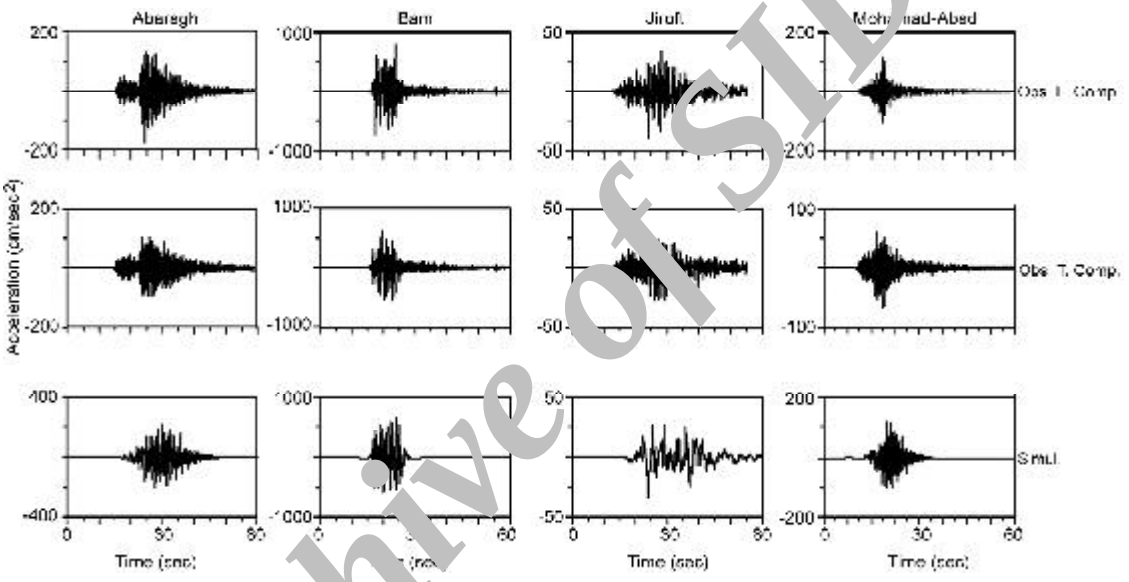

Figure 39. The observed horizontal acceleration and simulated records for model M1 based on NEIC solution.

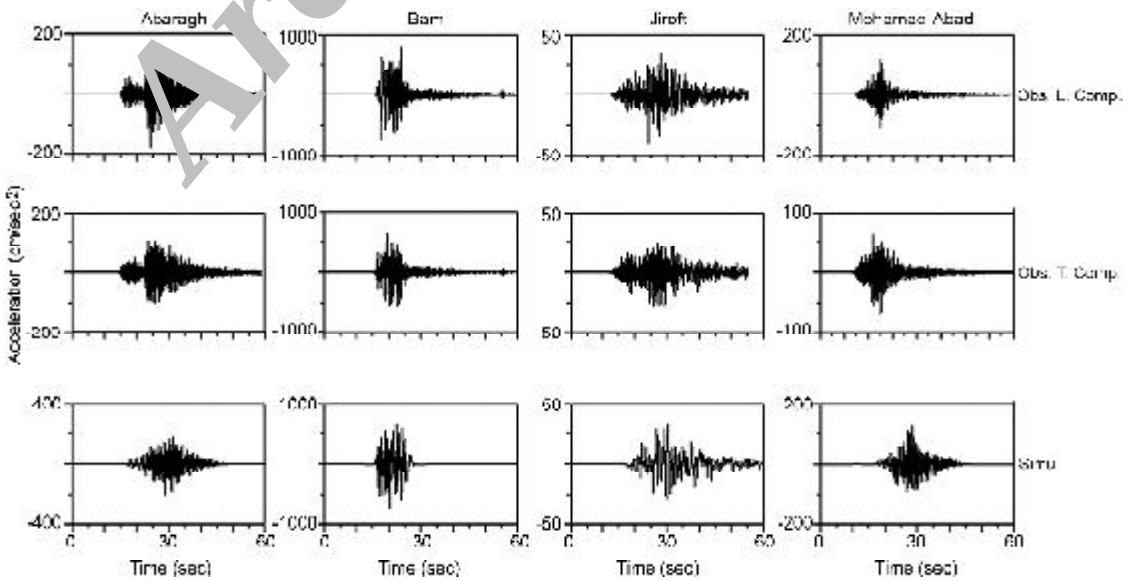

Figure 40. The observed horizontal acceleration and simulated records for model M2 based on HRV solution.

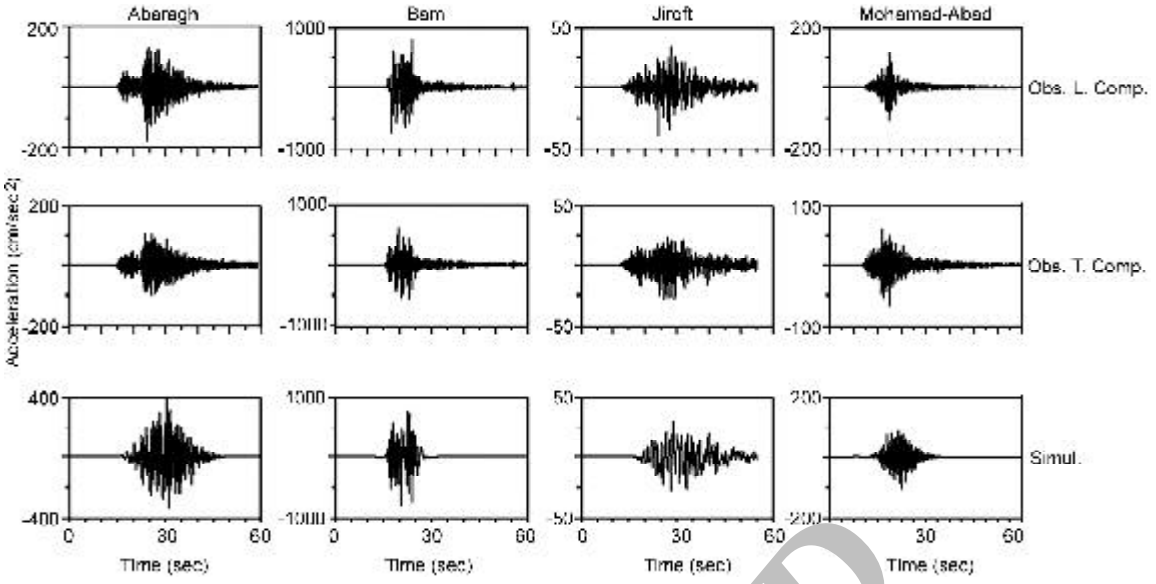

Figure 41. The observed horizontal acceleration and simulated records for model M3 based on analysis of SH-wave strong ground motion.

estimated peak ground acceleration and duration using Trifunac and Brady (1975) [?] for observed and simulated records for these three models at four stations are tabulated in Tables (5) and (6). The root mean square error (rmse) for 1, 2 and 3 sec between observed and simulated response spectra for these four stations are calculated using equation 3 and given in Table [illegible] for three different models of M_1, M_2 and M_3.

Table 4. Modeling parameters of rupture plane.

Modelling Parameters	
Length (km)	18 km [29]
Weight (km)	[illegible]
S-wave velocity	[illegible] km/s
Rupture velocity	[illegible]
Element dimension Number of element	3.6x2 25
Q= 194 $f^{0.77}$	[illegible]

Table 5. Observed and simulated peak ground acceleration for three models.

Station	Observed P.G.A (cm/sec^2)		Simulated P.G.A (cm/sec^2)		
	L	T	Model 1	Model 2	Model 3
Abaragh	162.6	107.7	217	204	194
Bam	775	623	663	747	804
Mohammad-Abad	120.1	71	118	124	104
Jiroft	39.6	27.3	34	32	29.4

Table 6. Observed and simulated duration for three models.

Station	Observed Duration (sec)		Simulated Duration (sec)		
	L	T	Model 1	Model 2	Model 3
Abaragh	15.3	19.2	14.0	14.6	14.6
Bam	8.0	9.7	8.0	8.3	8.3
Mohamad-Abad	13.5	22.4	13.0	12.9	12.9
Jiroft	23.2	25.9	20.6	21.5	21.5

7. Macroseismic Intensity and Isoseismal Maps

The north eastern parts of Bam were demolished more during the earthquake. The damage distribution map, (see Figure (42), *SERTIT* European satellite image), shows higher damages in the northern Bam, where it could be related to bad construction material and older building concentrated in these parts of the city. The higher damages in eastern Bam, however, could be related also to the near-fault conditions.

The isoseismal map of the Bam earthquake is prepared based on a field reconnaissance study [27] performed in the area immediately after the event, see Figure (43). Based on this study, the macroseismic intensity of the earthquake is estimated to be *IO=IX* (in *EMS*98 scale), where the strong motions and damaging effects seems to be attenuated very fast specially in the fault-normal direction. The intensity levels are estimated to be *VIII* in Baravat, *VII* in New-Arg (Arg-e Jadid) and airport area. The intensity level was estimated to be around IV-V in Kerman and Mahan.

8. Discussion

The Bam earthquake causes greatest human disaster in 2003 with more than 30000 victims and the demolishing the city of Bam. The 22 strong motion records obtained in this event are studied and six records were selected based on their high signal to noise ratio. The vertical and fault-normal (horizontal)

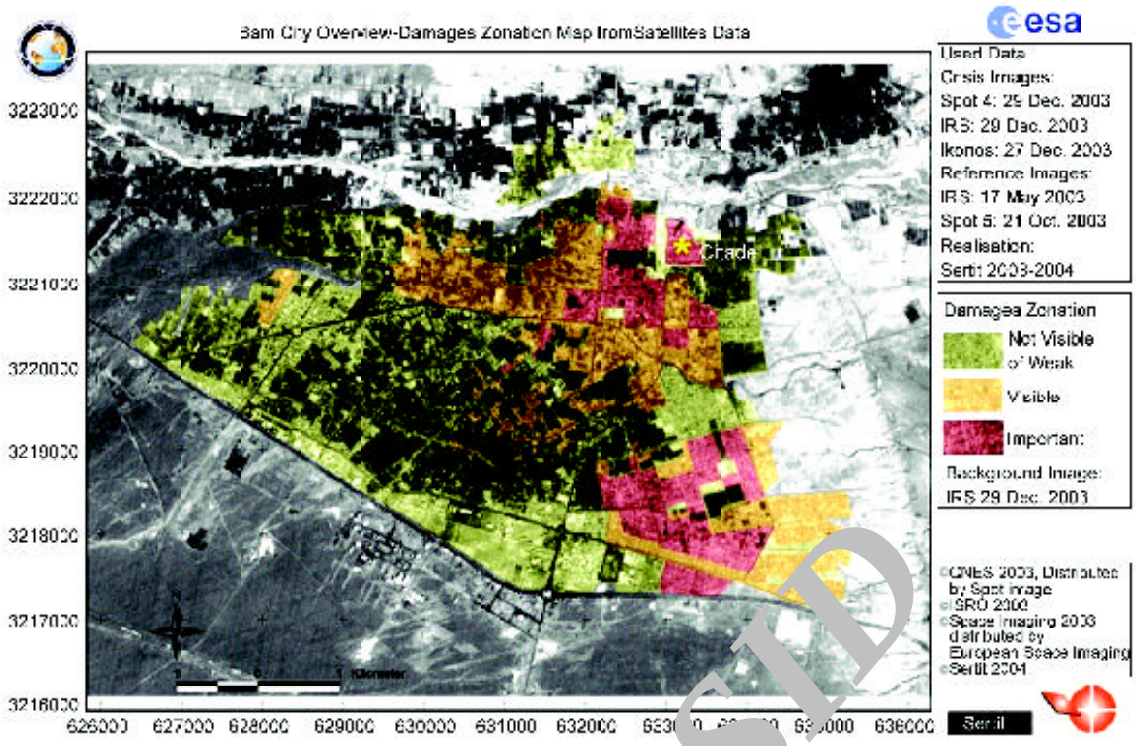

Figure 42. The damage zoning map estimated ESA using the SERTIT European satellite. The trace of the Bam fault scarp is shown by the author on the image. The red-shaded parts of the d are representative for the important damages where the brown and green parts are showing the moderate and low damages.

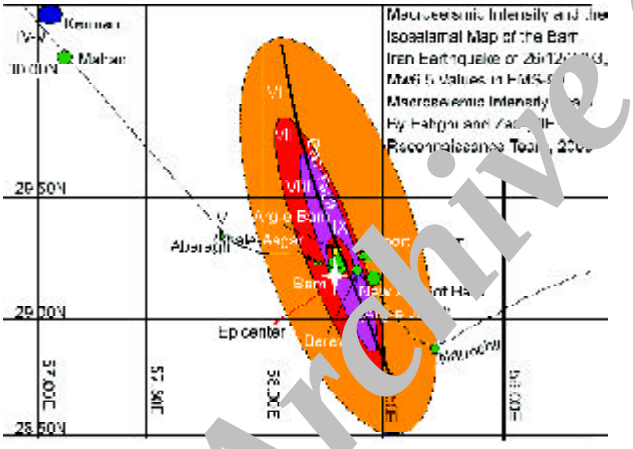

Figure 43. The isoseismal map prepared by the IIEES earthquake reconnaissance team [28]. The intensity values are given in EMS-98 scale.

directivity effects could be observed based on the greater damages along vertical and fault-normal horizontal directions, as well as the long period amplification in 5 to 10 seconds in the mainshock. Such effects are evident in the *H/V* ratios estimated for the Abaragh, Mohammadabad and Jiroft stations, see Figures (11), (12) and (13). These figures shows two major peaks for the *H/V* ratio at 0.1*Hz* and 0.6*Hz*. These two peaks could be related to the source directivity effects. The soil conditions in these stations probably did not lead to an amplification around 0.1*Hz*. The attenuation of strong motions in the fault normal direction was higher than in the fault-parallel direction and the attenuation rate was very high. The higher attenuation rate could be related to the high stress drop estimated for this event and low duration (about 10 seconds).

NEIC and *HRV* have analyzed far field broad band data to provide estimate of the strike, dip and rake for the 2003 Bam earthquake. *NEIC* suggest a strike, dip and rake of 174°, 88°, and 178°, while the *HRV* gives values of 173°, 63°, and 164°, respectively. It is noticed that the value of strike, dip and rake from these two studies are in fair agreement with the estimated strike, dip and rake from analysis of *SH* waves of recorded near field data, see Figure (38). Strong phases related to two sub-events have been identified on the strong ground motion data. It is observed that the causative fault for sub-event *S*1 has right-lateral strike slip mechanism, see Figure (38), while for *S*2 it is reverse mechanism with right-lateral strike-slip mechanism. The estimated location of sub-event *S*1 is at 58.30 and 29.02 at depth of 8*km* and it occurred 8 second before the sub-event *S*2. The sub-event *S*2 is located at 58.34 and 29.08 at depth of 8*km*. The high peak ground acceleration, which was observed at Bam station, can be explained by occurrence of the second sub-event with reverse mecha-

nism. The focal mechanisms of sub-events are determined on the basis of sparsely distributed accelerographs in relation to the overall size of the fault. Local strong ground motion records are generally known to be more sensitive to faulting of those sections of the fault closest to the station, while the more distant stations are unable to contribute suitable constraints for these sections of the fault. Meanwhile, the results obtained based on *SH*-wave analysis of strong ground motion for two sub-events are in fair agreements with the results obtained from waveform inversion of teleseismic data reported by Mostafazzde and Nalbant [28]. They also fond that the first sub-event had right-lateral strike-slip mechanism and second sub-event have reverse mechanism.

In the present study the rupture plane for Bam earthquake has been modeled using different parameters. Three models were considered based on *NEIC*, *HRV* and *SH*-wave analysis and acceleration time histories were simulated at four stations for which observation records were available. Comparison of simulated and observed records based on peak acceleration, duration and rms between observed and simulated response spectra indicate that model three is the preferred rupture model. This selection was done on the basis of two criteria:

(i) Maximum number of extracted features (peak ground acceleration and duration) showing less than 10% difference between observed and simulated observed for model *M*3 and

(ii) the preferred model gives maximum number of stations for which rmse is least between observed and simulated response spectra.

The peak ground acceleration and duration values for both observed and simulated records for the 2003 Bam earthquake are tabulated in Tables (5) and (6). Figure (44) shows distribution of these values with distance for model *M*3. In general, local topography, seismic source, propagation path and local site conditions will influence peak ground acceleration. It is observed that the values of peak ground acceleration at these stations are in fair agreement with observed values for model *M*3 compare to models *M*1 and *M*2. The distribution of simulated peak ground acceleration versus distance shows similar trends to observed peak ground acceleration.

The duration of simulated records are also in fair agreement with observed records. Again model 3 shows more match with observed compare to model *M*1 and model *M*2.

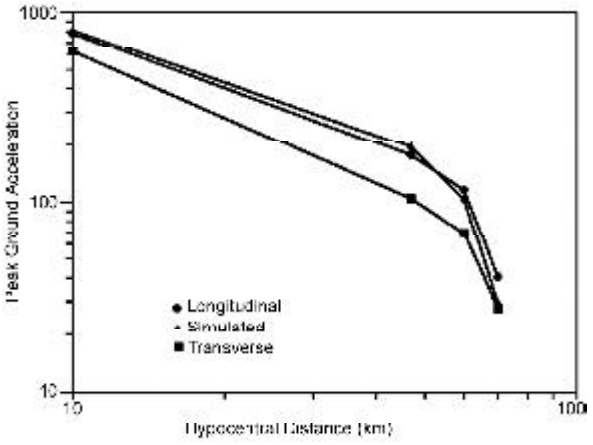

Figure 44. Comparison between observed peak horizontal acceleration and simulated peak acceleration for model M3

On the other hand the comparisons of root mean square error (*rmse*) at these four stations for three model shows that rmse error between observed and simulated response spectra is less for model *M*3 (see Table (7). Figure (45) shows response spectra for 5% damping for both horizontal components and simulated records for model *M*3. Comparison between observed and simulated records indicate that the rupture started at a depth of 8*km* and propagated from south toward Bam and north.

Table 7. Root mean square error between observed and simulated Response spectra for three models.

Model M1						
Station	Componet L			Componet T		
	1sec	2sec	3sec	1sec	2sec	3sec
Abaragh	3.70	4.30	4.20	5.50	6.50	6.50
Bam	0.60	0.62	0.63	0.91	0.92	0.92
Jiroft	0.33	0.39	0.49	1.09	1.01	1.03
Mohamad-Abad	0.59	0.56	1.28	0.58	0.74	2.2
Model M2						
Station	Componet L			Componet T		
Abaragh	2.19	0.50	2.46	3.25	3.49	3.91
Bam	0.82	0.84	0.84	0.84	0.82	0.82
Jiroft	0.48	0.46	0.45	1.52	1.45	1.53
Mohamad-Abad	0.62	0.98	1.03	0.63	1.37	1.57
Model M3						
Station	Componet L			Componet T		
Abaragh	1.90	1.80	1.70	2.90	2.70	2.60
Bam	0.30	0.40	0.41	0.70	0.68	0.65
Jiroft	0.29	0.29	0.39	0.38	0.41	0.62
Mohamad-Abad	0.62	0.61	0.59	0.96	0.88	0.88

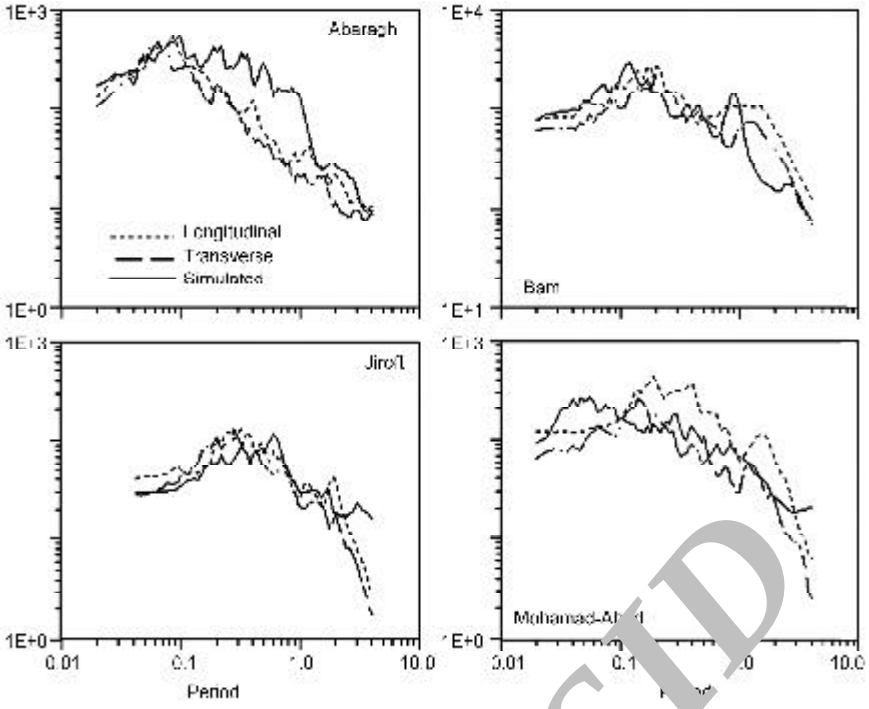

Figure 45. Comparison between observed and simulated [illegible] spectra for model M3.

9. Conclusion

The strong motions records and intensities observed in the Bam earthquake records are representative a very strong but short earthquake that had the large vertical and fault-normal near-fault effects. This earthquake had no visible surface fault displacement but some surface fissures created during the earthquake are observed along the Bam fault scarp. The shallow depth (8*km*) and the location of the epicenter near the city of Bam, along with the old and weak buildings caused the high levels of life and property losses during this event.

The following conclusions have emerged from the analysis of strong ground motion data for Bam earthquake:

- Although the duration of the strong motions in Bam was short (7 to 10 seconds), the long period (about 10 seconds) large amplitudes of the motions caused by the directivity effects in the fault-normal and vertical directions could be imagined as a continuations to the damage caused by this earthquake.
- The attenuation of strong motion was rapid. The rate of attenuation was even faster in the fault-normal direction (relative to the fault parallel direction).
- The Bam earthquake was a complex earthquake. The *SH*-wave accelerograms exhibited distinct phases corresponding to the energy released from two separate asperities.
- Two strong phases of energy are seen on the accelerograms. The first is interpreted to represent a starting sub-event with right-lateral strike slip mechanism and located south of Bam. The asperity corresponding to the second release of energy is interpreted to be released 8*sec* after first sub-event. The mechanism of the second sub-event is reverse mechanism.
- The ground motion indicates that the rupture started at a depth of 8*km* south of Bam and then propagated toward north. The high vertical peak acceleration in Bam station was due to occurrence of the second sub-event, which was located very close to the recording station.

Acknowledgment

We are grateful to Building and housing Research Center for providing the strong ground motion data that we analyzed here in this study. We are also thankful to Prof. Panza, Prof. Trifunac and all anonymous reviewer for their constructive comments on the manuscript.

References

1. Zaré, M. (2003). "Seismological Aspects of the Bam, SE Iran Earthquake of 26/12/2003, Mw 6.5", IIEES Web Site, http://www.iiees.ac.ir.

2. Ambraseys, N.N. and Melville, C.P. (1982). "A History of Persian Earthquakes", *Cambridge Earth Sci. Ser.*

3. National Earthquake Information Center (USGS), Web Site (2004). http:/neicr.usgs.gov.

4. United States Geological Survey, USGS, Digital Data Series DDS-62-C, 2001.

5. Harvard University, Seismology Department, Web Site (2004). http://www.seismology.harvard.edu, http://www.seismology.harvard.edu/

6. Haskell, N.A. (1964). "Total Energy and Energy Spectral Density of Elastic Wave Radiation from Propagating Faults", *Bull. Seism. Soc. of America*, **54**, 1811-1841.

7. Building and Housing Research Center (BHRC) (2004). http://www.bhrc.gov.ir/

8. Zaré, M., Bard,P-Y., Ghafory-Ashtiany, M. (1999). "Site Characterizations for the Iranian Strong Motion Network", Journal of Soil Dynamics and Earthquake Engineering, **18**(2), 101-121.

9. Arias, A. (1970). "A Measure of Earthquake Intensity", In Seismic Design of Nuclear Power Plants, R.J. Hansen Editor, M.I.T. press.

10. Housner, G.W. (1959). "Behavior of Structures During Earthquakes", *Journal of the Engineering Mechanics Division, ASCE*, **85**(EM14), 109-129.

11. Trifunac M.D. and Brady, A.G. (1975). "A Study on the Duration of the Strong Earthquake Ground Motions", *Bull. Seismol. Soc. of America*, **65**(3), 581-626.

12. Zaré, M. (1999). "Contribution à L'étude des Movements Forts en Iran: Du Catalogue Aux Lois D'atténuation", Université Joseph Fourier, Thése de Doctorat (Ph.D. Thesis), 237p.

13. Bard, P.-Y., Zare, M. and Ghafory-Ashtiany, M. (1998). "The Iranian Accelerometric Data Bank, A Revision and Data Correction", *Journal of Seismology and Earthquake Engineering*, **1**(1), 1-22.

14. Campos, J., Madariaga, R., Nabelek, J., Bukchin, B.G., Deschamps, A. (1994). "Faulting Process of the 1990 June 20 Iran Earthquake from Broad-Band Records", *Geophys. J. Int.*, **118**, 31-46.

15. Sarkar, I., Hamzehloo, H., and Khattri, K.N. (2003). Estimation of Causative Fault Parameters of the Rudbar Earthquake of June 20, 1990 from Near Field SH-Wave Data", *Tectonophysics*, **364**, 55-70.

16. Haskell, N.A. (1960). "Crustal Reflection of Plane SH Waves", *J. Geophys. Res.*, **65**, 4147-4150.

17. Aki, K. and Richards, P.G. (1980). "Quantitative Seismology", Theory and Methods, **1**, Freemn, San Francisco, 558p.

18. Lay, T. and Wallace, C. (1995). "Modern Global Seismology".

19. Somerville, P.G., Sen, M., and Cohee, B. (1991). "Simulation of Strong Ground Motion Recorded During the 1985 Michoacan, Mexico an Valparaiso, Chile Earthquakes", *Bull. Seismol. Soc. Am.*, **81**, 1-27.

20. Brune, J.N. (1970). "Tectonic Stree and Spectra of Seismic Shear Waves from Earthquakes", *J. Geophys. Res.*, **75**, 4997-5009.

21. Boore, D.M. (1983). "Stochastic Simulation of High-Frequency Ground Motions Based on Seismological Models of the Radiated Spectra, *Bull. Seismol. Soc. Am.*, **73**, 1865-1894.

22. Atkinson, G. and Boore, D.M. (1995). "Ground-Motion Relations for Eastern North America", *Bull. Seism. Soc. Am.*, **85**, 17-30.

23. Atkinson, G. and Boore, D.M. (1998). "Evaluation of Models for Earthquake Source in Eastern North America", *Bull. Seismol. Soc. Am.*, **88**, 917-934.

24. Atkinson, G., Silva, (1997). An Empirical Study of Earthquake Source Spectra for Californian Earthquakes, *Bull. Seismol. Soc. Am.*, **87**, 97-113.

25. Safak, E. (1988). "Analytical Approach to Calulation of Response Spectra from Seismological Models of Ground Motion", *Earthquake Engineering Struct. Dyn.*, **16**, 121-134.

26. Irikura, K. (1986). "Prediction of Strong Ground Acceleration Motions Using Empirical Green's Function", *Proc. 7th Japan Earthquake Engineering Symp.*, 151-157.

27. Eshghi, S., Zare, M., Naser-Asadi, K., Seyed-Razzaghi, M., Noorali-Ahari, M., and Motamedi, M. (2004). Reconnaissance Report on 26 Dec. 2003 Bam Earthquake, International Institute of

Earthquake Engineering and Seismology (IIEES), Report in Persian.

28. Mostafazadeh, M. and Nalbant, S. (2004). "Waveform Inversion of 26 December 2003, Bam Earthquake", *J. Seismol. Earthquake Engineering* (Submitted).

29. Wells, D.L. and Coppersmith, K.J. (1994). "New Empirical Relationships Among Magnitude, Rupture length, Rupture Width, Rupture Area, and Surface Displacement, *Bull. Seismol. Soc. Am.*, **84**, 974-1002.

30. Farahbod, M. and Alahyarkhani, M. (2003). "Attenuation and Propagation Characteristics of Seismic Waves in Iran", *Proc. 4th Int. Conf. Earthq. Engg.*, Tehran, I.R. Iran.